INSTITUTE OF PHYSICS PUBLISHING JOURNAL OF PHYSICS B: ATOMIC, MOLECULAR AND OPTICAL PHYSICS

J. Phys. B: At. Mol. Opt. Phys. **37** (2004) 247–281 PII: S0953-4075(04)67802-3

Electron impact excitation of the argon $3p^5 4s$ configuration: differential cross-sections and cross-section ratios

M A Khakoo[1], P Vandeventer[1], J G Childers[1], I Kanik[2], C J Fontes[3], K Bartschat[4], V Zeman[5], D H Madison[6], S Saxena[7], R Srivastava[7] and A D Stauffer[8]

[1] Department of Physics, California State University, Fullerton, CA 92834, USA
[2] Jet Propulsion Laboratory, California Institute of Technology, Pasadena, CA 91109, USA
[3] Applied Theoretical and Computational Physics Division, Los Alamos National Laboratory, Los Alamos, NM 87545, USA
[4] Department of Physics and Astronomy, Drake University, Des Moines, IA 50311, USA
[5] Department of Chemistry, University of Toronto, Toronto, ON, M5S 3H6, Canada
[6] Department of Physics, University of Missouri, Rolla, MO 65401, USA
[7] Department of Physics, Indian Institute of Technology Roorkee, Roorkee-247667, India
[8] Department of Physics and Astronomy, York University, Toronto, ON, M3J 1P3, Canada

Received 16 August 2003
Published 9 December 2003
Online at stacks.iop.org/JPhysB/37/247 (DOI: 10.1088/0953-4075/37/1/016)

Abstract

New electron-impact differential cross-section (DCS) and DCS ratio measurements for the excitation of the four levels making up the $3p^5 4s$ configuration of argon are reported at incident electron energies of 14, 15, 17.5, 20, 30, 50 and 100 eV. These cross-sections were obtained using a conventional high resolution electron spectrometer. Elastic electron scattering from argon was used as a calibration standard. Electron–helium DCSs were used to determine the instrumental transmission of the spectrometer. Further checks of the relative shape of these DCS measurements were made using the method of gas mixtures (Ne mixed with Ar). We also present results from new calculations of these DCSs using the *R*-matrix method, the unitarized first-order many-body theory, the semi-relativistic distorted-wave Born approximation, and the relativistic distorted-wave method. Comparison with available experimental DCSs and DCS ratios is also presented.

1. Introduction

The excitation of the ground np^6 state of heavy noble gases to the first excited-electron $np^5(n+1)s$ configuration results in the excitation of four levels. The collective study of these excitations has been shown to constitute a unique system where differential cross-sections (DCSs) and their ratios provide valuable insights on relativistic interactions, which

contribute to the electron scattering dynamics (Guo *et al* 1999). We recently carried out an investigation of the electron impact excitation of this configuration in Ne (Khakoo *et al* 2002) and observed some encouraging agreement between our measurements and theory, but many more questions regarding the disagreements were left open. Here we extend our previous work to experimental DCSs and DCS ratios (r, r', r'') (Guo *et al* 1999) for the excitation of Ar from the $3p^6$ ground-state configuration to the first-excited $3p^54s$ configuration. A detailed comparison with available theoretical models is also presented. The four levels comprising the Ar $3p^54s$ listed, with increasing energy above the ground state, are $(3p^54s)[3/2]^o_2$, $(3p^54s)[3/2]^o_1$, $(3p^54s')[1/2]^o_0$ and $(3p^54s')[1/2]^o_1$, following the $j[K]_J$ coupling scheme (Khakoo *et al* 2002).

Previous measurements (integral and differential inelastic cross-sections) for the excitation of the $3p^54s$ configuration of Ar are summarized by Filipovic *et al* (2000a, 2000b) who have most recently measured DCSs for electron impact excitation of the $(3p^54s')[1/2]^o_1$ level (as well as the $(3p^54p)[1/2]^e_1$ and $(3p^54p')[1/2]^e_0$ levels which are not considered in the present work) at the incident electron energies (E_0) of 16, 20, 30, 40, 50 and 80 eV. They also measured DCSs for the $(3p^54s)[3/2]^o_1$ level at 20, 40, 50 and 80 eV, and for the metastable $(3p^54s)[3/2]^o_2$ and $(3p^54s')[1/2]^o_0$ levels at 20 and 40 eV. The data in Filipovic *et al* (2000a, 2000b) were obtained for a range of scattering angles (θ) from 5° to 150°. There also exist the DCS measurements by Chutjian and Cartwright (1981) for all four levels at 16, 20, 30, 50 and 100 eV and θ values of 5–138°. The measurements of Filipovic *et al* (2000a, 2000b) were normalized to experimental elastic electron–Ar scattering DCSs of Srivastava *et al* (1981) and Panajotovic *et al* (1997), and those of Chutjian and Cartwright (1981) were normalized to the experimental elastic electron–Ar scattering DCSs of Srivastava *et al* (1981). Recently, a semi-relativistic distorted-wave Born calculation by Madison *et al* (1998) compared well with the DCSs of Chutjian and Cartwright (1981) at E_0 values of 30, 50 and 100 eV, but showed that there was considerable room for overall improvement.

Additionally, McConkey and co-workers (Corr *et al* 1991, 1992, Khakoo and McConkey 1987, 1986) and Becker and co-workers (Zheng and Becker 1993, Martus *et al* 1991) have measured polarization–correlation parameters for the excitation of the $(3p^54s)[3/2]^o_1$ and $(3p^54s')[1/2]^o_1$ levels from the ground state level at 25, 40, 50, 60 and 80 eV using electron–photon coincidence methods. These data were restricted to scattering angles $\theta < 55°$ because of experimental statistics. Reasonable agreement with the distorted-wave Born approximation (DWBA, Bartschat and Madison 1987), first-order many-body theory (FOMBT, Meneses *et al* 1985, 1991) and relativistic distorted wave approximation (RDWA, Zuo *et al* 1992) for P_1, P_2 and P_3 polarization parameters was observed at these small angles. From these results and from observation of the P_4 polarization (see the review in Becker *et al* 1992), it was inferred that Ar essentially displayed LS-coupled behaviour. Using spin-polarized electrons, Dümmler *et al* (1995) measured inelastic left–right asymmetries (S_A) for electron impact excitation of the $(3p^54s)[3/2]^o_1$ and $(3p^54s')[1/2]^o_1$ levels at $E_0 = 15$, 25, 30 and 40 eV. The results were compared to the DWBA (Bartschat and Madison 1987) and RDWA (Zuo *et al* 1992) with mixed agreements. For excellent summaries of these experiments see Becker *et al* (1992) and Andersen and Bartschat (2001).

The present DCS and cross-section ratio measurements cover the more extensive range of E_0 of 14, 15, 17.5, 20, 30, 50 and 100 eV and a θ range of 2–135° in mostly 5° intervals for $\theta > 5°$. The DCSs were normalized to the elastic DCSs of Srivastava *et al* (1981), Panajotovic *et al* (1997), Furst *et al* (1989), Dubois and Rudd (1976), Andrick (see Furst *et al* 1989) and Williams (1979). A selective average was taken for those sets of elastic DCSs that showed agreement within their error bars.

Additionally, we present our new semi-relativistic 41-state R-matrix calculations (RM41), semi-relativistic unitarized first-order many-body theory (UFOMBT), semi-relativistic first-order DWBA and RDWA calculations using a single-configuration ground-state (SCGS-RDWA), and compare these to the experimental measurements. For the UFOMBT, a single configuration was used to compute the excited state wavefunctions with the Cowan structure code. However, a nine-configuration calculation was also carried out to gauge the relative importance of configuration interaction (see below). As mentioned, for the RDWA single-configuration ground-state wavefunctions (SCGS-RDWA) were used. Additional 5-state R-matrix calculations (RM5 and RM5a) are also presented. These were performed either with the original CIV3 (Hibbert 1975) wavefunctions (RM5) or a revised structure description (RM5a) in which the intermediate-coupling mixing coefficients α and β (see below) were adjusted to agree with those obtained from optical oscillator strength (OOS) measurements (Chan *et al* 1992). For the DWBA, the calculations used the same 5-state wavefunctions that were used in the R-matrix RM5a calculations with the adjusted values of α and β. For a detailed description of these models, see Khakoo *et al* (2002), Hibbert (1975), Bartschat and Zeman (1999) and the references therein.

Bartschat and Madison (1992) and Guo *et al* (1999) have highlighted the use of DCS ratios as an alternative set of parameters for probing scattering dynamics. These ratios can be determined more accurately and readily than DCSs or coherence parameters, and provide substantial tests of theoretical models. DCS ratios for the first excited configuration of Ar are defined as follows:

$$r = \frac{\mathrm{DCS}(4\mathrm{s}[3/2]^{\mathrm{o}}_2)}{\mathrm{DCS}(4\mathrm{s}'[1/2]^{\mathrm{o}}_0)}, \qquad r' = \frac{\mathrm{DCS}(4\mathrm{s}[3/2]^{\mathrm{o}}_1)}{\mathrm{DCS}(4\mathrm{s}'[1/2]^{\mathrm{o}}_1)} \qquad \text{and} \qquad r'' = \frac{\mathrm{DCS}(4\mathrm{s}[3/2]^{\mathrm{o}}_2)}{\mathrm{DCS}(4\mathrm{s}[3/2]^{\mathrm{o}}_1)}. \quad (1)$$

In the single-configuration representation, the $3p^5 4s$ levels in Ar can be expressed in the intermediate-coupling scheme (see e.g. Bartschat and Madison 1987) in terms of LS-coupled wavefunctions $|\phi\rangle$ as

$$\begin{aligned} &|4\mathrm{s}[3/2]^{\mathrm{o}}_2\rangle = |4\ {}^3\mathrm{P}_2\rangle, \\ &|4\mathrm{s}[3/2]^{\mathrm{o}}_1\rangle = \alpha|4\ {}^3\mathrm{P}_1\rangle + \beta|4\ {}^1\mathrm{P}_1\rangle, \\ &|4\mathrm{s}'[1/2]^{\mathrm{o}}_0\rangle = |4\ {}^3\mathrm{P}_0\rangle \qquad \text{and} \\ &|4\mathrm{s}'[1/2]^{\mathrm{o}}_1\rangle = \alpha|4\ {}^1\mathrm{P}_1\rangle - \beta|4\ {}^3\mathrm{P}_1\rangle. \end{aligned} \quad (2)$$

Here α and β are the intermediate-coupling (unitary) mixing coefficients, i.e., $\alpha^2 + \beta^2 = 1$. The values of (α, β) obtained from the Cowan code (single-configuration model) used by the UFOMBT, from the CIV3 code used by the R-matrix (RM41 and RM5) calculations and from the GRASP code used by the SCGS-RDWA, are (0.893, 0.450), (0.95, 0.31) and (0.894, 0.449), respectively. We note the SCGS-RDWA and the UFOMBT calculations used very similar values for the (α, β) coefficients. A semi-empirical approach was used in Cowan's code to obtain (α, β) values that are similar to those inferred from the high-resolution, OOS electron–electron coincidence measurements by Chan *et al* (1992), whereas the SCGS-RDWA coefficients were obtained from an *ab initio* calculation (Parpia *et al* 1996). Mixing coefficients associated with additional configurations typically are at least an order of magnitude smaller as can be seen from the Cowan (*ab initio*) five-configuration results in table 1. These *ab initio* results contain inaccurate (α, β) coefficients and are provided for relative comparisons only. The (semi-empirical) single-configuration data also displayed in this table were actually used in the UFOMBT excitation calculations. We also note that the (α, β) parameters used in the RM5 and RM5a calculations were (0.950, 0.310) and (0.893, 0.450), respectively.

From equations (1) and (2), we see that r involves excitation to optically-forbidden levels excitable essentially via spin-exchange. In the limiting case of degenerate fine-structure levels

Table 1. Mixing coefficients for the $3p^5 4s$ configuration of Ar taken from the Cowan code. The left-hand side shows *ab initio*, five-configuration results and the right-hand side shows the semi-empirical, single-configuration results. The single-configuration calculation was used in the present UFOMBT calculations.

State	Amplitude	Core	Valence	LS term	Amplitude	Core	Valence	LS term
$3p^6[0]_0$	1.00E+00	$(\ldots 3p^6)^1S$		$3\,^1S_0$	1.00E+00	$(\ldots 3p^6)^1S$		$3\,^1S_0$
$3p^5 4s[3/2]^o_2$	2.08E−08	$(\ldots 3s^2 3p^5)^2P$	$(3d^1)^2D$	$4\,^3F_2$				
	−9.33E−04	$(\ldots 3s^2 3p^5)^2P$	$(3d^1)^2D$	$4\,^3D_2$				
	3.85E−02	$(\ldots 3s^2 3p^5)^2P$	$(3d^1)^2D$	$4\,^3P_2$				
	7.61E−04	$(\ldots 3s^2 3p^5)^2P$	$(3d^1)^2D$	$4\,^1D_2$				
	9.99E−01	$(\ldots 3s^2 3p^5)^2P$	$(4s^1)^2S$	$4\,^3P_2$	1.00E+00	$(\ldots 3s^2 3p^5)^2P$	$(4s^1)^2S$	$4\,^3P_2$
	4.13E−09	$(\ldots 3s^2 3p^5)^2P$	$(4d^1)^2D$	$4\,^3F_2$				
	−3.74E−04	$(\ldots 3s^2 3p^5)^2P$	$(4d^1)^2D$	$4\,^3D_2$				
	1.99E−02	$(\ldots 3s^2 3p^5)^2P$	$(4d^1)^2D$	$4\,^3P_2$				
	3.05E−04	$(\ldots 3s^2 3p^5)^2P$	$(4d^1)^2D$	$4\,^1D_2$				
	8.02E−03	$(\ldots 3s^2 3p^5)^2P$	$(5s^1)^2S$	$4\,^3P_2$				
	3.76E−03	$(\ldots 3s^2 3p^5)^2P$	$(6s^1)^2S$	$4\,^3P_2$				
	−1.89E−02	$(\ldots 3s^1 3p^6)^2S$	$(4p^1)^2P$	$4\,^3P_2$				
	6.51E−11	$(\ldots 3s^1 3p^6)^2S$	$(4d^1)^2F$	$4\,^3F_2$				
	−8.14E−03	$(\ldots 3s^1 3p^6)^2S$	$(5p^1)^2P$	$4\,^3P_2$				
	5.01E−11	$(\ldots 3s^1 3p^6)^2S$	$(5f^1)^2F$	$4\,^3F_2$				
$3p^5 4s[3/2]^o_1$	−9.35E−04	$(\ldots 3s^2 3p^5)^2P$	$(3d^1)^2D$	$4\,^3D_1$				
	3.46E−02	$(\ldots 3s^2 3p^5)^2P$	$(3d^1)^2D$	$4\,^3P_1$				
	1.13E−02	$(\ldots 3s^2 3p^5)^2P$	$(3d^1)^2D$	$4\,^1P_1$				
	8.61E−01	$(\ldots 3s^2 3p^5)^2P$	$(4s^1)^2S$	$4\,^3P_1$	8.93E−01	$(\ldots 3p^5)^2P$	$(4s^1)^2S$	$4\,^3P_1$
	5.07E−01	$(\ldots 3s^2 3p^5)^2P$	$(4s^1)^2S$	$4\,^1P_1$	4.50E−01	$(\ldots 3p^5)^2P$	$(4s^1)^2S$	$4\,^1P_1$
	−3.63E−04	$(\ldots 3s^2 3p^5)^2P$	$(4d^1)^2D$	$4\,^3D_1$				
	1.78E−02	$(\ldots 3s^2 3p^5)^2P$	$(4d^1)^2D$	$4\,^3P_1$				
	5.48E−03	$(\ldots 3s^2 3p^5)^2P$	$(4d^1)^2D$	$4\,^1P_1$				
	6.52E−03	$(\ldots 3s^2 3p^5)^2P$	$(5s^1)^2S$	$5\,^3P_1$				
	−9.44E−03	$(\ldots 3s^2 3p^5)^2P$	$(5s^1)^2S$	$5\,^1P_1$				
	3.10E−03	$(\ldots 3s^2 3p^5)^2P$	$(6s^1)^2S$	$6\,^3P_1$				
	−4.65E−03	$(\ldots 3s^2 3p^5)^2P$	$(6s^1)^2S$	$6\,^1P_1$				
	−1.64E−02	$(\ldots 3s^1 3p^6)^2S$	$(4p^1)^2P$	$4\,^3P_1$				
	−7.91E−03	$(\ldots 3s^1 3p^6)^2S$	$(4p^1)^2P$	$4\,^1P_1$				
	−7.04E−03	$(\ldots 3s^1 3p^6)^2S$	$(5p^1)^2P$	$5\,^3P_1$				
	−3.18E−03	$(\ldots 3s^1 3p^6)^2S$	$(5p^1)^2P$	$5\,^1P_1$				
$3p^5 4s'[1/2]^o_0$	4.27E−02	$(\ldots 3s^2 3p^5)^2P$	$(3d^1)^2D$	$4\,^3P_0$				
	9.99E−01	$(\ldots 3s^2 3p^5)^2P$	$(4s^1)^2S$	$4\,^3P_0$	1.00E+00	$(\ldots 3s^2 3p^5)^2P$	$(4s^1)^2S$	$4\,^3P_0$
	2.16E−02	$(\ldots 3s^2 3p^5)^2P$	$(4d^1)^2D$	$4\,^3P_0$				
	8.07E−03	$(\ldots 3s^2 3p^5)^2P$	$(5s^1)^2S$	$5\,^3P_0$				
	3.79E−03	$(\ldots 3s^2 3p^5)^2P$	$(6s^1)^2S$	$6\,^3P_0$				
	−1.92E−02	$(\ldots 3s^1 3p^6)^2S$	$(4p^1)^2P$	$4\,^3P_0$				
	−8.22E−03	$(\ldots 3s^1 3p^6)^2S$	$(5p^1)^2P$	$5\,^3P_0$				
$3p^5 4s'[1/2]^o_1$	−1.61E−04	$(\ldots 3s^2 3p^5)^2P$	$(3d^1)^2D$	$4\,^3D_1$				
	−2.25E−02	$(\ldots 3s^2 3p^5)^2P$	$(3d^1)^2D$	$4\,^3P_1$				
	2.17E−02	$(\ldots 3s^2 3p^5)^2P$	$(3d^1)^2D$	$4\,^1P_1$				
	−5.07E−01	$(\ldots 3s^2 3p^5)^2P$	$(4s^1)^2S$	$4\,^3P_1$	−4.50E−01	$(\ldots 3p^5)^2P$	$(4s^1)^2S$	$4\,^3P_1$
	8.61E−01	$(\ldots 3s^2 3p^5)^2P$	$(4s^1)^2S$	$4\,^1P_1$	8.93E−01	$(\ldots 3p^5)^2P$	$(4s^1)^2S$	$4\,^1P_1$
	−4.69E−05	$(\ldots 3s^2 3p^5)^2P$	$(4d^1)^2D$	$4\,^3D_1$				
	−1.13E−02	$(\ldots 3s^2 3p^5)^2P$	$(4d^1)^2D$	$4\,^3P_1$				

Table 1. (Continued.)

State	Amplitude	Core	Valence	*LS* term	Amplitude	Core	Valence	*LS* term
	1.02E−02	$(\ldots 3s^2 3p^5)^2P$	$(4d^1)^2D$	$4\,^1P_1$				
	−4.91E−03	$(\ldots 3s^2 3p^5)^2P$	$(5s^1)^2S$	$5\,^3P_1$				
	−1.77E−02	$(\ldots 3s^2 3p^5)^2P$	$(5s^1)^2S$	$5\,^1P_1$				
	−2.22E−03	$(\ldots 3s^2 3p^5)^2P$	$(6s^1)^2S$	$6\,^3P_1$				
	−8.51E−03	$(\ldots 3s^2 3p^5)^2P$	$(6s^1)^2S$	$6\,^1P_1$				
	9.77E−03	$(\ldots 3s^1 3p^6)^2S$	$(4p^1)^2P$	$4\,^3P_1$				
	−1.36E−02	$(\ldots 3s^1 3p^6)^2S$	$(4p^1)^2P$	$4\,^1P_1$				
	4.20E−03	$(\ldots 3s^1 3p^6)^2S$	$(5p^1)^2P$	$5\,^3P_1$				
	−5.46E−03	$(\ldots 3s^1 3p^6)^2S$	$(5p^1)^2P$	$5\,^1P_1$				

(Bartschat and Madison 1987), r attains its LS coupling limit of 5, i.e., *the statistical weight ratio of the respective* ($J = 2$ and 0) levels. Apart from non-degeneracy effects (prevalent close to threshold), deviations from the statistical weight ratio of 5 can indicate the presence of spin–orbit coupling interactions between the continuum (scattering) electron and the target electron(s) or the presence of second-order effects in the excitation of the target (Khakoo *et al* 1994). The ratio r' involves excitations to the optically-allowed $J = 1$ levels. However, these $J = 1$ levels have mixed triplet–singlet LS character. In the optical limit (high E_0 and small θ), application of dipole selection rules show, within the single-configuration coupling scheme, a limit for r':

$$\text{Dipole limit } r' = \beta^2/\alpha^2. \tag{3}$$

Deviation from the optical limit could indicate either the importance of the triplet part of the $J = 1$ components or the need for mixing from higher-lying configurations in the model to accurately describe these levels. On the other hand, if only pure spin-exchange excitation of these levels occurs, only the $|^3P\rangle$ LS-component in equation (2) is excited, and then the limit for r' is

$$\text{Exchange limit } r' = \alpha^2/\beta^2. \tag{4}$$

Thus the r' parameter serves as a very useful qualitative indicator. Note that using the Cowan code values, $r' \cong 4$ in the exchange limit and $r' \cong 0.254$ in the dipole limit. The third parameter r'' provides additional information on the coupling scheme needed to describe the metastable, optically-forbidden levels *relative* to the optically-allowed levels, and consequently completes the framework of these ratios. Ratio measurements not only provide accurate values for comparison with theoretical models, but also tests of the target wavefunctions used in these models as well as the treatment of scattering dynamics (Khakoo *et al* 2002).

2. Experimental details

Unlike our previous Ne work (Khakoo *et al* 2002) only one spectrometer was used in this work. The set-up for this high-resolution spectrometer has been discussed previously (Khakoo *et al* 2002) so only a brief summary will be given here. The apparatus consisted of an electron energy-loss spectrometer with double hemispherical energy selectors in both the gun and the analyser sections as has been detailed in Guo *et al* (1999). The spectrometer was housed in a vacuum chamber pumped with a 12-inch diffusion pump. The base pressure of the vacuum chamber was $\approx 1 \times 10^{-7}$ Torr. Both the gun and the analyser sections were baked to $>120\,^\circ$C during the experiment to maintain the stable conditions necessary for taking electron energy-loss spectra over long periods. To reduce the earth's magnetic field the vacuum chamber was

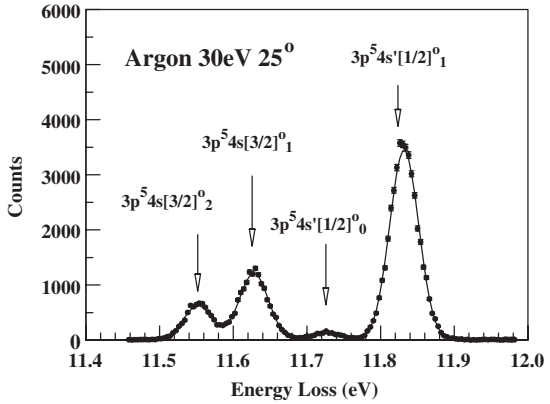

Figure 1. Electron energy-loss spectrum of Ar taken at $E_0 = 30$ eV and $\theta = 25°$ showing the pertinent level features which comprise the excitation of the $3p^5 4s$ configuration from the ground state. The solid curve is our unfolding fit using Gaussian-synthesized line profiles. See the text for a further description.

shielded with two doubly-layered high-permeability, low-field and low-permeability, high-field μ-metal shields. The inner double layer shield was further demagnetized using a 0–100 A AC-driven coil (coupled to a variable transformer) between the μ-metal layers, and thus the magnetic field in the chamber could be reduced to below 2 mG. An important feature of this spectrometer is the absence of 'wings' in the instrumental energy profile often seen in spectrometers with single hemispherical analysers (e.g. that used in Khakoo *et al* 2002). This characteristic enabled us to resolve the weak metastable energy-loss features from the stronger dipole-allowed transitions in Ar. The spectrometer operated at an energy resolution of 40–60 meV (FWHM) with an incident electron current ranging from 5 to 30 nA. The spectrometer could observe scattered electrons at scattering angles up to 130°. This apparatus was computer-controlled to enable efficient data acquisition. The computer processed the multi-channel scaling measurement of the energy-loss scan, controlled the scattering angle positioning, monitored the pressure behind the gas line and modulated the gas beam via a thin molybdenum beam flag. Contact potential measurements using the He^- $1s2s^2$ resonance enabled us to calibrate our incident energy to well within ± 0.05 eV. Operating at high resolution, spectra in the inelastic energy-loss range of 11.4–12.0 eV were taken at the above E_0 values, and unfolded to determine DCSs of the individual levels. Analysis of the measured spectra was done off-line. A well-tested multi-Gaussian unfolding program (Khakoo *et al* 1994) was used to unfold the spectra. The energies of the levels of Ar from Moore's spectroscopy tables (Moore 1952) were used in the unfolding program. A typical electron energy-loss spectrum of Ar with typical unfolding is shown in figure 1. Characteristic reduced chi-squared (χ^2_ν) values of the fits to the spectra were in the range of 1–3. The separated intensities of the individual features of the Ar levels were used directly to calculate the ratios in equation (1). Several spectra were taken at each angle to check reproducibility and to improve statistics.

Thereafter, with an increased incident electron current (20–30 nA), but lower energy resolution, elastic and 11.4–12.0 eV electron energy-loss spectra were obtained. The molybdenum flag was again used to chop the gas beam to enable the determination of the background scattering in the experiment. We note that the chopper introduced a small smooth secondary electron background. To determine the gas-related background, the smooth

backgrounds from the chopper-out and chopper-in were removed from the corresponding energy-loss spectra, and then the modified chopper-in spectrum was subtracted from the chopper-out spectrum. Care was also taken to make sure that this background was minimized so that in the worst case the elastic scattering peak was not contaminated by more than 5% of this background. Following a set of elastic–inelastic measurements, with the analyser tuning left unchanged Ar was removed and He was introduced into the collision region and, at $E_0 = 31.7$ eV, an elastic–inelastic energy-loss spectrum of He covering the energy-loss (E_L) range $E_L < 0$ to $E_L > E_0$ was taken and used to determine the transmission of the analyser as described by Nickel *et al* (1989). We have observed in recent measurements in our laboratory (Childers *et al* 2003) that the ionization continuum is a flat profile (within 10%) at the scattering angle of 90°. From the inelastic/elastic ratio (corrected for transmission), we determined the DCSs for excitation of the summed $3p^5 4s$ configuration of Ar. As stated previously, we used the absolute elastic DCSs of Furst *et al* (1989), Andrick (given in Furst *et al* 1989), Srivastava *et al* (1981), Dubois and Rudd (1976), Williams (1979) and Panajotovic *et al* (1997) for normalization. For $E_0 > 20$ eV the Ar elastic DCSs exhibit (unfortunately in this case) deep minima typically around scattering angles of 60° and 120°. Normalizing to the elastic DCS around these minima resulted in differential inelastic DCSs that varied considerably and whose behaviour was not reproducible. Therefore, for θ within 30° of these minima, we measured spectra of a mixture of Ar and Ne at roughly equal pressures and then carried out the method of mixtures, described in Khakoo *et al* (2002), by measuring the intensity of the summed $2p^5 3s$ and $3p^5 4s$ configurations of Ne and Ar. The inelastic DCSs of Ne in Khakoo *et al* (2002) were used to determine relative DCSs of the Ar excitation and therefore accurately establish the shape of the DCS curve around these minima. At lower E_0 values, the inelastic DCSs could be reproduced easily. In all cases, spectra were repeated to check the reproducibility of the inelastic DCSs, and the experiment was kept running until reproducibility was achieved, in most cases, in triplicate.

The relative intensities obtained from the high-resolution spectra were summed and normalized directly to the summed absolute DCSs determined above. The present experimental data (summed and individual level DCSs) are summarized in tables 2(a)–(g). Table 3 summarizes the sources of uncertainties in our measurements.

3. Results and discussion

3.1. Summed DCSs

Using the above procedures, we carried out measurements of the DCSs for the individual levels making up the $3p^5 4s$ configuration of Ar at E_0 values of 14, 15, 17.5, 20, 30, 50 and 100 eV for θ in the range of 5–130°. These DCSs and corresponding ratios are compared to our new calculations.

Figures 2(a)–(g) show our summed experimental and theoretical DCSs for the electron impact excitation of the $3p^6 \rightarrow 3p^5 4s$ configuration of Ar at the E_0 and θ values discussed above. At $E_0 = 14$ eV, figure 2(a), very good agreement is observed with the SCGS theory. There is no perceptible difference between the 5-state R-matrix calculations without (RM5) and with (RM5a) experimentally corrected (α, β) parameters. The 41-state R-matrix model does not do as well as the 5-state R-matrix approach, which is in better qualitative agreement with the measurements. The DWBA gives an excellent shape, but is about 60% higher in magnitude than the experiment. The UFOMBT does not show good agreement. At this energy only the R-matrix model based on a close-coupling-type expansion would be expected to be valid.

At $E_0 = 15$ eV, figure 2(b), disagreements between the R-matrix calculations continue and overall agreement between experiment and theory is unsatisfactory. We note the significantly

Table 2. Normalized experimental DCSs and DCS ratios at different E_0 values for the summed and individual levels of the $3p^5 4s$ configuration of Ar. The second column under each heading corresponds to ± 1 standard deviation estimated uncertainties. (a) $E_0 = 14$ eV, (b) $E_0 = 15$ eV, (c) $E_0 = 17.5$ eV, (d) $E_0 = 20$ eV, (e) $E_0 = 30$ eV, (f) $E_0 = 50$ eV and (g) $E_0 = 100$ eV. DCS units: $cm^2\ sr^{-1}$.

(a) 14 eV argon

θ (deg)	Sum	Error	$3p^5 4s[3/2]^o_2$	Error	$3p^5 4s[3/2]^o_1$	Error	$3p^5 4s'[1/2]^o_0$	Error
10	3.27E−18	4.2E−19	4.20E−19	6.6E−20	8.22E−19	1.2E−19	4.67E−20	1.6E−20
15	3.19E−18	4.1E−19	4.71E−19	6.4E−20	7.84E−19	1.1E−19	6.36E−20	1.1E−20
20	2.88E−18	3.7E−19	4.88E−19	6.8E−20	7.11E−19	9.9E−20	6.72E−20	1.3E−20
25	2.62E−18	3.3E−19	4.58E−19	6.5E−20	6.64E−19	9.3E−20	5.34E−20	1.1E−20
30	2.36E−18	3.0E−19	4.66E−19	6.5E−20	6.14E−19	8.3E−20	6.09E−20	1.1E−20
35	2.14E−18	2.7E−19	4.78E−19	6.8E−20	5.20E−19	7.3E−20	4.80E−20	9.9E−21
40	1.92E−18	2.5E−19	4.27E−19	6.4E−20	4.89E−19	7.2E−20	7.71E−20	1.5E−20
45	1.79E−18	2.3E−19	4.10E−19	6.1E−20	4.64E−19	6.9E−20	6.14E−20	1.2E−20
50	1.47E−18	1.9E−19	3.88E−19	5.9E−20	3.82E−19	5.8E−20	3.83E−20	8.9E−21
55	1.32E−18	1.7E−19	3.51E−19	5.4E−20	3.48E−19	5.4E−20	3.51E−20	8.6E−21
60	1.17E−18	1.5E−19	3.22E−19	5.1E−20	3.14E−19	4.9E−20	3.95E−20	9.5E−21
65	1.05E−18	1.3E−19	3.27E−19	5.4E−20	2.56E−19	4.3E−20	5.47E−20	1.2E−20
70	9.69E−19	1.2E−19	3.19E−19	5.5E−20	2.76E−19	4.7E−20	4.01E−20	1.2E−20
75	8.62E−19	1.1E−19	3.06E−19	5.8E−20	2.36E−19	4.3E−20	6.08E−20	1.5E−20
80	8.31E−19	1.1E−19	3.26E−19	5.1E−20	2.25E−19	3.4E−20	3.48E−20	8.0E−21
85	7.41E−19	9.5E−20	2.77E−19	4.2E−20	1.97E−19	2.9E−20	4.37E−20	8.3E−21
90	8.13E−19	1.0E−19	3.00E−19	4.7E−20	2.33E−19	3.6E−20	4.04E−20	9.0E−21
95	8.54E−19	1.1E−19	2.83E−19	4.5E−20	2.35E−19	3.8E−20	3.57E−20	8.6E−21
100	9.76E−19	1.2E−19	3.21E−19	4.7E−20	2.80E−19	4.1E−20	4.63E−20	8.9E−21
105	1.29E−18	1.7E−19	4.18E−19	6.4E−20	3.36E−19	5.2E−20	6.66E−20	1.3E−20
110	1.34E−18	1.7E−19	4.05E−19	5.9E−20	3.47E−19	5.2E−20	4.16E−20	9.2E−21
115	1.53E−18	2.0E−19	4.33E−19	6.4E−20	3.80E−19	5.6E−20	5.28E−20	1.1E−20
120	1.61E−18	2.1E−19	4.41E−19	6.7E−20	3.95E−19	6.0E−20	6.03E−20	1.3E−20
125	1.65E−18	2.1E−19	4.51E−19	6.7E−20	4.29E−19	6.4E−20	6.84E−20	1.4E−20
130	1.59E−18	2.0E−19	4.52E−19	9.6E−20	3.40E−19	8.3E−20	7.83E−20	2.9E−20

θ (deg)	$3p^5 4s'[1/2]^o_1$	Error	r	Error	r'	Error	r''	Error
10	1.97E−18	2.8E−19	8.69E+00	9.5E+00	4.32E−01	3.3E−02	4.76E−01	9.0E−02
15	1.86E−18	2.5E−19	7.48E+00	2.1E+00	4.19E−01	2.0E−02	6.05E−01	5.0E−02
20	1.59E−18	2.2E−19	8.69E+00	3.6E+00	4.65E−01	2.9E−02	7.26E−01	5.4E−02
25	1.43E−18	2.0E−19	1.07E+01	6.2E+00	4.55E−01	2.1E−02	6.91E−01	7.7E−02
30	1.21E−18	1.6E−19	8.51E+00	3.5E+00	5.28E−01	1.0E−02	7.38E−01	6.4E−02
35	1.09E−18	1.5E−19	8.72E+00	2.3E+00	4.77E−01	1.5E−02	9.08E−01	7.1E−02
40	9.28E−19	1.3E−19	5.53E+00	7.1E−01	5.27E−01	1.1E−02	8.73E−01	3.6E−02
45	8.52E−19	1.2E−19	7.13E+00	2.1E+00	5.46E−01	2.6E−02	8.94E−01	7.6E−02
50	6.60E−19	9.8E−20	1.01E+01	1.8E+00	5.79E−01	1.6E−02	1.02E+00	4.4E−02
55	5.76E−19	8.8E−20	6.97E+00	1.7E+00	5.62E−01	3.7E−02	1.06E+00	7.3E−02
60	4.88E−19	7.5E−20	7.71E+00	3.3E+00	6.32E−01	5.0E−02	1.02E+00	6.2E−02
65	4.12E−19	6.7E−20	1.16E+01	2.4E+01	6.00E−01	7.2E−02	1.25E+00	1.1E−01
70	3.34E−19	5.6E−20	1.47E+01	4.2E+01	7.67E−01	9.4E−02	1.23E+00	2.0E−01
75	2.60E−19	4.6E−20	5.04E+00	9.3E−01	9.09E−01	3.4E−02	1.30E+00	9.6E−02
80	2.35E−19	3.6E−20	9.69E+00	3.5E+00	1.01E+00	2.9E−02	1.39E+00	1.2E−01
85	2.08E−19	3.1E−20	6.59E+00	2.1E+00	9.83E−01	6.5E−02	1.37E+00	1.2E−01
90	2.09E−19	3.3E−20	8.33E+00	3.6E+00	1.23E+00	1.1E−01	1.27E+00	8.0E−02
95	2.80E−19	4.4E−20	8.81E+00	3.3E+00	8.61E−01	5.8E−02	1.22E+00	1.0E−01

Table 2. (Continued.)

θ (deg)	$3p^5 4s'[1/2]^o_1$	Error	r	Error	r'	Error	r''	Error
100	3.12E−19	4.6E−20	6.80E+00	2.4E+00	9.76E−01	8.8E−02	1.15E+00	9.7E−02
105	4.56E−19	6.9E−20	7.70E+00	9.3E+00	8.02E−01	1.2E−01	1.26E+00	1.7E−01
110	5.42E−19	7.9E−20	1.11E+01	5.2E+00	6.36E−01	4.9E−02	1.21E+00	8.8E−02
115	6.50E−19	9.5E−20	7.58E+00	2.2E+00	5.74E−01	3.8E−02	1.14E+00	5.9E−02
120	6.86E−19	1.0E−19	7.22E+00	2.7E+00	5.66E−01	3.3E−02	1.20E+00	1.3E−01
125	6.88E−19	1.0E−19	7.38E+00	2.8E+00	5.93E−01	5.0E−02	1.13E+00	9.8E−02
130	7.17E−19	1.5E−19	5.77E+00	1.8E+00	4.75E−01	5.8E−02	1.33E+00	1.7E−01

(b) 15 eV argon

θ (deg)	Sum	Error	$3p^5 4s[3/2]^o_2$	Error	$3p^5 4s[3/2]^o_1$	Error	$3p^5 4s'[1/2]^o_0$	Error
5	1.10E−17	1.3E−18						
8								
10	8.00E−18	9.5E−19	5.02E−19	8.5E−20	1.96E−18	2.6E−19	1.14E−19	5.1E−20
15	5.98E−18	7.1E−19	5.67E−19	7.3E−20	1.52E−18	1.9E−19	1.39E−19	2.5E−20
20	4.19E−18	5.0E−19	5.71E−19	8.0E−20	1.06E−18	1.3E−19	9.84E−20	3.1E−20
25	3.14E−18	3.7E−19	4.75E−19	6.3E−20	7.56E−19	9.5E−20	9.71E−20	1.9E−20
30	2.57E−18	3.1E−19	4.41E−19	6.1E−20	6.24E−19	8.1E−20	4.96E−20	2.0E−20
35	2.29E−18	2.7E−19	4.41E−19	5.7E−20	5.60E−19	7.2E−20	8.47E−20	1.8E−20
40	2.22E−18	2.6E−19	4.68E−19	5.8E−20	5.58E−19	6.9E−20	9.26E−20	1.5E−20
45	2.17E−18	2.6E−19	5.00E−19	6.4E−20	5.49E−19	7.0E−20	1.06E−19	1.7E−20
50	2.28E−18	2.7E−19	5.68E−19	7.1E−20	5.49E−19	6.8E−20	9.86E−20	1.5E−20
55	2.22E−18	2.6E−19	5.43E−19	7.0E−20	5.60E−19	7.2E−20	1.05E−19	1.7E−20
60	2.50E−18	3.0E−19	6.44E−19	7.9E−20	6.07E−19	7.5E−20	1.29E−19	1.8E−20
65	2.64E−18	3.1E−19	7.24E−19	9.3E−20	6.76E−19	8.6E−20	1.09E−19	1.9E−20
70	2.54E−18	3.0E−19	7.25E−19	9.2E−20	6.39E−19	8.1E−20	1.34E−19	2.0E−20
75	2.41E−18	2.9E−19	7.70E−19	1.0E−19	6.40E−19	8.5E−20	1.26E−19	2.4E−20
80	1.84E−18	2.2E−19	6.17E−19	8.2E−20	4.77E−19	6.3E−20	1.15E−19	1.9E−20
85	1.62E−18	1.9E−19	5.75E−19	8.1E−20	4.11E−19	5.7E−20	1.07E−19	2.0E−20
90	1.46E−18	1.7E−19	5.30E−19	7.3E−20	3.99E−19	5.4E−20	9.46E−20	1.8E−20
95	1.59E−18	1.9E−19	5.35E−19	6.9E−20	4.30E−19	5.5E−20	1.05E−19	1.7E−20
100	1.83E−18	2.2E−19	5.88E−19	7.7E−20	4.77E−19	6.2E−20	1.10E−19	1.8E−20
105	2.25E−18	2.7E−19	6.45E−19	8.1E−20	6.03E−19	7.6E−20	1.29E−19	1.8E−20
110	2.62E−18	3.1E−19	7.48E−19	9.4E−20	6.53E−19	8.2E−20	1.34E−19	2.0E−20
115	3.17E−18	3.8E−19	8.45E−19	1.0E−19	8.00E−19	9.9E−20	1.64E−19	2.3E−20
120	3.59E−18	4.3E−19	9.09E−19	1.1E−19	9.09E−19	1.1E−19	1.67E−19	2.4E−20
125	3.83E−18	4.5E−19	9.31E−19	1.1E−19	9.41E−19	1.2E−19	1.99E−19	2.7E−20
130	3.86E−18	4.6E−19	9.57E−19	1.2E−19	9.64E−19	1.2E−19	1.77E−19	2.4E−20

θ (deg)	$3p^5 4s'[1/2]^o_1$	Error	r	Error	r'	Error	r''	Error
5								
8			1.04E+01	1.2E+01	3.08E−01	1.2E−02	2.01E−01	2.6E−02
10	5.42E−18	7.0E−19	4.40E+00	1.9E+00	3.61E−01	1.4E−02	2.56E−01	3.0E−02
15	3.75E−18	4.6E−19	4.09E+00	5.6E−01	4.05E−01	1.7E−03	3.73E−01	1.6E−02
20	2.45E−18	3.1E−19	5.75E+00	1.8E+00	4.31E−01	7.6E−03	5.29E−01	3.5E−02
25	1.81E−18	2.3E−19	4.89E+00	7.4E−01	4.17E−01	2.6E−03	6.28E−01	2.8E−02
30	1.46E−18	1.9E−19	2.09E+01	3.1E+01	4.28E−01	1.0E−02	7.07E−01	4.2E−02
35	1.20E−18	1.5E−19	5.00E+00	9.1E−01	4.62E−01	1.4E−02	7.82E−01	2.9E−02
40	1.10E−18	1.4E−19	4.87E+00	5.9E−01	5.08E−01	1.2E−02	8.31E−01	1.8E−02

Table 2. (Continued.)

θ (deg)	$3p^5 4s'[1/2]^o_1$	Error	r	Error	r'	Error	r''	Error
45	1.02E−18	1.3E−19	4.69E+00	4.8E−01	5.38E−01	1.3E−02	9.11E−01	1.6E−02
50	1.06E−18	1.3E−19	5.41E+00	5.5E−01	5.08E−01	1.1E−02	1.04E+00	2.1E−02
55	1.01E−18	1.3E−19	5.15E+00	5.1E−01	5.54E−01	1.3E−02	9.70E−01	1.5E−02
60	1.12E−18	1.4E−19	5.00E+00	3.0E−01	5.43E−01	9.1E−03	1.06E+00	8.6E−03
65	1.13E−18	1.5E−19	6.65E+00	7.9E−01	5.97E−01	1.4E−02	1.07E+00	1.8E−02
70	1.05E−18	1.3E−19	5.43E+00	4.4E−01	6.11E−01	1.4E−02	1.13E+00	1.3E−02
75	8.77E−19	1.2E−19	6.18E+00	8.6E−01	7.26E−01	2.4E−02	1.21E+00	3.3E−02
80	6.33E−19	8.4E−20	5.37E+00	5.6E−01	7.54E−01	2.1E−02	1.29E+00	3.6E−02
85	5.32E−19	7.5E−20	5.37E+00	6.9E−01	7.72E−01	2.5E−02	1.40E+00	5.0E−02
90	4.39E−19	6.0E−20	5.60E+00	7.5E−01	9.10E−01	3.1E−02	1.33E+00	5.0E−02
95	5.20E−19	6.8E−20	5.11E+00	4.9E−01	8.26E−01	2.1E−02	1.24E+00	3.2E−02
100	6.49E−19	8.5E−20	5.29E+00	5.1E−01	7.46E−01	2.0E−02	1.23E+00	2.8E−02
105	8.72E−19	1.1E−19	5.02E+00	3.3E−01	6.92E−01	1.4E−02	1.07E+00	1.0E−02
110	1.09E−18	1.4E−19	5.57E+00	4.1E−01	6.00E−01	1.2E−02	1.15E+00	1.2E−02
115	1.36E−18	1.7E−19	5.14E+00	3.6E−01	5.86E−01	1.1E−02	1.06E+00	1.2E−02
120	1.60E−18	2.0E−19	5.47E+00	3.9E−01	5.76E−01	1.0E−02	9.91E−01	8.8E−03
125	1.76E−18	2.2E−19	4.67E+00	2.6E−01	5.35E−01	8.2E−03	9.89E−01	5.9E−03
130	1.76E−18	2.2E−19	5.47E+00	3.3E−01	5.48E−01	8.2E−03	9.94E−01	1.4E−02

(c) 17.5 eV argon

θ (deg)	Sum	Error	$3p^5 4s[3/2]^o_2$	Error	$3p^5 4s[3/2]^o_1$	Error	$3p^5 4s'[1/2]^o_0$	Error
3								
5	1.83E−17	2.4E−18	2.29E−19	6.0E−20	4.19E−18	5.6E−19	9.25E−20	1.2E−20
8								
10	9.85E−18	1.3E−18	3.24E−19	5.3E−20	2.34E−18	3.1E−19	1.40E−20	2.8E−20
15	6.66E−18	8.6E−19	3.36E−19	5.3E−20	1.49E−18	2.0E−19	7.98E−20	2.7E−20
20	4.23E−18	5.4E−19	2.62E−19	4.3E−20	9.81E−19	1.4E−19	3.02E−20	2.2E−20
25	2.94E−18	3.8E−19	3.78E−19	5.0E−20	6.71E−19	8.8E−20	5.81E−20	1.0E−20
30	2.26E−18	2.9E−19	3.75E−19	5.0E−20	5.40E−19	7.1E−20	7.89E−20	1.2E−20
35	2.09E−18	2.7E−19	4.16E−19	5.5E−20	5.17E−19	6.8E−20	7.69E−20	1.2E−20
40	2.32E−18	3.0E−19	4.90E−19	6.5E−20	5.69E−19	7.5E−20	9.54E−20	1.4E−20
45	2.47E−18	3.2E−19	4.80E−19	6.4E−20	5.70E−19	7.6E−20	9.56E−20	1.3E−20
50	2.73E−18	3.5E−19	5.63E−19	7.3E−20	6.64E−19	8.6E−20	1.10E−19	1.5E−20
55	2.98E−18	3.8E−19	6.55E−19	8.7E−20	7.07E−19	9.3E−20	1.22E−19	1.7E−20
60	3.66E−18	4.7E−19	8.38E−19	1.1E−19	9.16E−19	1.2E−19	1.65E−19	2.3E−20
65	4.15E−18	5.4E−19	1.02E−18	1.3E−19	9.90E−19	1.3E−19	1.87E−19	2.5E−20
70	3.89E−18	5.0E−19	1.01E−18	1.3E−19	9.73E−19	1.3E−19	2.01E−19	2.7E−20
75	2.58E−18	3.3E−19	7.75E−19	1.0E−19	6.34E−19	8.3E−20	1.49E−19	2.0E−20
80	1.78E−18	2.3E−19	5.60E−19	7.3E−20	4.50E−19	5.9E−20	1.09E−19	1.5E−20
85	1.47E−18	1.9E−19	4.93E−19	6.5E−20	3.72E−19	4.9E−20	9.11E−20	1.2E−20
90	1.22E−18	1.6E−19	4.05E−19	5.3E−20	3.21E−19	4.2E−20	8.25E−20	1.1E−20
95	1.22E−18	1.6E−19	3.64E−19	4.8E−20	3.07E−19	4.1E−20	7.47E−20	1.1E−20
100	1.38E−18	1.8E−19	4.11E−19	5.4E−20	3.43E−19	4.5E−20	8.19E−20	1.1E−20
105	1.71E−18	2.2E−19	4.00E−19	5.3E−20	4.08E−19	5.4E−20	8.03E−20	1.1E−20
110	2.14E−18	2.8E−19	4.92E−19	6.4E−20	5.32E−19	7.0E−20	1.01E−19	1.4E−20
115	2.70E−18	3.5E−19	5.55E−19	7.3E−20	6.34E−19	8.3E−20	1.17E−19	1.6E−20
120	3.31E−18	4.3E−19	6.90E−19	9.1E−20	7.84E−19	1.0E−19	1.45E−19	2.0E−20
125	3.46E−18	4.4E−19	6.86E−19	9.0E−20	8.31E−19	1.1E−19	1.43E−19	1.9E−20
130	3.28E−18	4.2E−19	6.69E−19	8.8E−20	7.71E−19	1.0E−19	1.33E−19	1.8E−20

Table 2. (Continued.)

θ (deg)	$3p^5 4s'[1/2]^o_1$	Error	r	Error	r'	Error	r''	Error
3			1.14E+00	1.3E+00	2.92E−01	8.9E−03	2.98E−02	3.4E−02
5	1.39E−17	1.9E−18	2.47E+00	5.6E−01	3.02E−01	7.4E−03	5.48E−02	1.2E−02
8			3.39E+00	2.4E+00	3.23E−01	8.4E−03	7.45E−02	1.6E−02
10	7.18E−18	9.5E−19	3.80E+00	4.7E+01	3.25E−01	6.5E−03	1.39E−01	1.4E−02
15	4.75E−18	6.3E−19	4.21E+00	1.4E+00	3.14E−01	7.8E−03	2.25E−01	1.9E−02
20	2.95E−18	4.0E−19	5.66E+00	6.3E+00	3.32E−01	1.0E−02	2.67E−01	2.6E−02
25	1.84E−18	2.4E−19	7.10E+00	1.6E+00	3.66E−01	5.4E−03	5.77E−01	2.3E−02
30	1.26E−18	1.7E−19	4.72E+00	7.7E−01	4.24E−01	7.4E−03	6.93E−01	2.7E−02
35	1.08E−18	1.4E−19	5.32E+00	5.5E−01	4.74E−01	7.4E−03	7.60E−01	1.0E−02
40	1.17E−18	1.5E−19	5.19E+00	5.3E−01	4.87E−01	9.2E−03	8.62E−01	1.5E−02
45	1.32E−18	1.7E−19	5.03E+00	2.7E−01	4.31E−01	7.0E−03	8.42E−01	2.1E−02
50	1.39E−18	1.8E−19	5.18E+00	3.0E−01	4.78E−01	8.4E−03	8.48E−01	2.2E−02
55	1.49E−18	2.0E−19	5.36E+00	2.6E−01	4.73E−01	7.1E−03	9.25E−01	2.0E−02
60	1.74E−18	2.3E−19	5.09E+00	2.1E−01	5.26E−01	7.5E−03	9.14E−01	1.9E−02
65	1.93E−18	2.5E−19	5.66E+00	3.0E−01	5.06E−01	6.0E−03	1.03E+00	1.0E−02
70	1.70E−18	2.2E−19	5.06E+00	2.4E−01	5.73E−01	7.3E−03	1.05E+00	1.2E−02
75	1.03E−18	1.3E−19	5.19E+00	2.3E−01	6.17E−01	9.2E−03	1.22E+00	1.4E−02
80	6.65E−19	8.7E−20	5.13E+00	2.0E−01	6.78E−01	1.1E−02	1.24E+00	2.1E−02
85	5.11E−19	6.7E−20	5.52E+00	3.6E−01	7.32E−01	1.4E−02	1.32E+00	2.3E−02
90	4.15E−19	5.5E−20	4.97E+00	2.9E−01	7.74E−01	1.2E−02	1.26E+00	1.9E−02
95	4.74E−19	6.3E−20	4.87E+00	2.3E−01	6.48E−01	8.9E−03	1.19E+00	1.2E−02
100	5.38E−19	7.1E−20	5.03E+00	2.8E−01	6.34E−01	1.0E−02	1.20E+00	1.2E−02
105	8.23E−19	1.1E−19	4.99E+00	2.3E−01	4.96E−01	5.2E−03	9.81E−01	4.7E−03
110	1.01E−18	1.3E−19	4.90E+00	2.5E−01	5.25E−01	7.7E−03	9.24E−01	1.4E−02
115	1.39E−18	1.8E−19	4.75E+00	2.1E−01	4.55E−01	6.3E−03	8.76E−01	1.8E−02
120	1.69E−18	2.2E−19	4.75E+00	1.9E−01	4.64E−01	6.4E−03	8.79E−01	1.8E−02
125	1.80E−18	2.3E−19	4.90E+00	3.2E−01	4.58E−01	9.0E−03	8.20E−01	2.4E−02
130	1.71E−18	2.2E−19	5.05E+00	1.7E−01	4.52E−01	5.4E−03	8.68E−01	1.5E−02

(d) 20 eV argon

θ (deg)	Sum	Error	$3p^5 4s[3/2]^o_2$	Error	$3p^5 4s[3/2]^o_1$	Error	$3p^5 4s'[1/2]^o_0$	Error
2								
5	2.06E−17	2.1E−18	9.02E−19	9.5E−20	4.70E−18	4.9E−19	1.90E−19	2.3E−20
6								
7								
8								
10	1.44E−17	1.5E−18	9.22E−19	9.9E−20	3.35E−18	3.5E−19	2.08E−19	2.6E−20
15	8.96E−18	9.3E−19	8.61E−19	9.2E−20	2.10E−18	2.2E−19	1.65E−19	1.9E−20
20	6.00E−18	6.1E−19	8.13E−19	8.9E−20	1.43E−18	1.5E−19	1.53E−19	2.0E−20
25	4.58E−18	4.7E−19	8.48E−19	8.8E−20	1.08E−18	1.1E−19	1.68E−19	1.9E−20
30	3.53E−18	3.6E−19	7.47E−19	7.7E−20	8.39E−19	8.7E−20	1.47E−19	1.6E−20
35	3.15E−18	3.2E−19	6.71E−19	7.2E−20	7.50E−19	8.0E−20	1.26E−19	1.5E−20
40	2.77E−18	2.8E−19	5.47E−19	5.8E−20	6.60E−19	6.9E−20	1.14E−19	1.3E−20
45	2.85E−18	2.9E−19	5.18E−19	5.6E−20	6.74E−19	7.3E−20	1.03E−19	1.2E−20
50	2.51E−18	2.6E−19	4.40E−19	4.8E−20	5.71E−19	6.2E−20	8.68E−20	1.0E−20
55	2.36E−18	2.4E−19	4.02E−19	4.5E−20	5.43E−19	6.0E−20	8.02E−20	1.0E−20
60	2.24E−18	2.3E−19	4.16E−19	4.6E−20	5.12E−19	5.6E−20	7.92E−20	9.4E−21
65	2.13E−18	2.4E−19	4.52E−19	5.5E−20	5.00E−19	6.0E−20	7.98E−20	1.1E−20
70	1.86E−18	2.3E−19	4.15E−19	5.3E−20	4.52E−19	5.7E−20	8.75E−20	1.2E−20
75	1.71E−18	1.9E−19	4.27E−19	5.0E−20	4.05E−19	4.7E−20	8.63E−20	1.1E−20

Table 2. (Continued.)

θ (deg)	Sum	Error	$3p^5 4s[3/2]^o_2$	Error	$3p^5 4s[3/2]^o_1$	Error	$3p^5 4s'[1/2]^o_0$	Error
80	1.45E−18	1.6E−19	3.80E−19	4.4E−20	3.61E−19	4.2E−20	7.57E−20	9.5E−21
85	1.25E−18	1.4E−19	3.57E−19	4.0E−20	3.03E−19	3.4E−20	7.46E−20	8.7E−21
90	1.27E−18	1.4E−19	3.75E−19	4.3E−20	3.16E−19	3.6E−20	6.85E−20	8.2E−21
95	1.11E−18	1.2E−19	3.22E−19	3.8E−20	2.63E−19	3.2E−20	6.67E−20	8.9E−21
100	1.12E−18	1.2E−19	2.97E−19	3.3E−20	2.57E−19	2.9E−20	6.26E−20	7.3E−21
105	1.33E−18	1.4E−19	3.25E−19	3.6E−20	3.05E−19	3.3E−20	6.72E−20	7.7E−21
110	1.67E−18	1.8E−19	3.72E−19	4.5E−20	3.77E−19	4.5E−20	7.53E−20	1.0E−20
115	2.41E−18	2.5E−19	4.81E−19	5.2E−20	5.59E−19	6.1E−20	1.14E−19	1.3E−20
120	2.85E−18	3.0E−19	5.38E−19	5.9E−20	6.56E−19	7.2E−20	1.19E−19	1.4E−20
125	3.55E−18	3.7E−19	6.72E−19	7.2E−20	8.19E−19	8.8E−20	1.56E−19	1.8E−20
130	3.91E−18	4.0E−19	7.25E−19	7.8E−20	9.12E−19	9.7E−20	1.62E−19	1.8E−20

θ (deg)	$3p^5 4s'[1/2]^o_1$	Error	r	Error	r'	Error	r''	Error
2			3.49E+00	3.6E−01	3.10E−01	2.9E−03	1.12E−01	4.5E−03
5	1.48E−17	1.5E−18	4.73E+00	4.2E−01	3.18E−01	3.9E−03	1.92E−01	6.6E−03
6			3.80E+00	4.1E−01	3.28E−01	5.2E−03	2.01E−01	9.0E−03
7			4.47E+00	4.8E−01	3.32E−01	5.2E−03	2.35E−01	9.5E−03
8			4.88E+00	7.1E−01	3.28E−01	5.6E−03	2.49E−01	1.2E−02
10	9.95E−18	1.0E−18	4.45E+00	4.5E−01	3.38E−01	5.4E−03	2.75E−01	1.1E−02
15	5.84E−18	6.1E−19	5.25E+00	4.9E−01	3.60E−01	4.2E−03	4.09E−01	1.3E−02
20	3.61E−18	3.8E−19	5.32E+00	4.4E−01	3.96E−01	3.9E−03	5.70E−01	1.6E−02
25	2.49E−18	2.6E−19	5.11E+00	4.9E−01	4.27E−01	4.0E−03	7.68E−01	1.8E−02
30	1.80E−18	1.9E−19	5.04E+00	3.0E−01	4.66E−01	6.1E−03	8.95E−01	6.5E−03
35	1.60E−18	1.7E−19	5.18E+00	3.3E−01	4.61E−01	6.3E−03	8.68E−01	7.0E−03
40	1.45E−18	1.5E−19	4.82E+00	3.0E−01	4.54E−01	3.9E−03	8.30E−01	1.1E−02
45	1.55E−18	1.7E−19	5.06E+00	3.6E−01	4.30E−01	9.7E−03	7.72E−01	2.6E−02
50	1.41E−18	1.5E−19	5.07E+00	2.9E−01	4.04E−01	7.8E−03	7.72E−01	2.2E−02
55	1.33E−18	1.5E−19	5.01E+00	3.3E−01	4.07E−01	8.8E−03	7.40E−01	2.5E−02
60	1.23E−18	1.3E−19	5.25E+00	2.8E−01	4.15E−01	7.2E−03	8.13E−01	2.1E−02
65	1.10E−18	1.3E−19	5.67E+00	3.8E−01	4.57E−01	1.0E−02	9.04E−01	3.0E−02
70	9.07E−19	1.1E−19	4.74E+00	2.8E−01	5.00E−01	8.6E−03	9.17E−01	2.5E−02
75	7.97E−19	9.2E−20	4.96E+00	3.1E−01	5.07E−01	1.1E−02	1.06E+00	3.1E−02
80	6.36E−19	7.3E−20	5.02E+00	2.7E−01	5.68E−01	1.2E−02	1.05E+00	2.9E−02
85	5.09E−19	5.7E−20	4.68E+00	2.2E−01	6.01E−01	9.9E−03	1.16E+00	2.6E−02
90	5.10E−19	5.8E−20	5.53E+00	3.1E−01	6.15E−01	1.3E−02	1.19E+00	2.8E−02
95	4.62E−19	5.4E−20	4.83E+00	3.1E−01	5.70E−01	1.6E−02	1.22E+00	3.6E−02
100	5.00E−19	5.5E−20	4.74E+00	2.8E−01	5.14E−01	1.4E−02	1.15E+00	4.0E−02
105	6.31E−19	6.8E−20	4.90E+00	3.0E−01	4.85E−01	1.2E−02	1.06E+00	3.5E−02
110	8.50E−19	1.0E−19	4.94E+00	3.7E−01	4.43E−01	1.3E−02	9.88E−01	4.0E−02
115	1.25E−18	1.3E−19	4.18E+00	3.2E−01	4.49E−01	9.4E−03	8.64E−01	3.3E−02
120	1.54E−18	1.7E−19	4.51E+00	3.3E−01	4.27E−01	1.1E−02	8.18E−01	3.0E−02
125	1.91E−18	2.0E−19	4.39E+00	1.7E−01	4.31E−01	2.4E−03	8.08E−01	1.2E−02
130	2.11E−18	2.2E−19	4.48E+00	1.7E−01	4.32E−01	2.3E−03	7.95E−01	1.2E−02

(e) 30 eV argon

θ (deg)	Sum	Error	$3p^5 4s[3/2]^o_2$	Error	$3p^5 4s[3/2]^o_1$	Error	$3p^5 4s'[1/2]^o_0$	Error
3								
5	1.09E−16	1.6E−17	1.25E−18	1.8E−19	2.42E−17	3.5E−18	2.82E−19	4.2E−20
8								
10	5.88E−17	8.3E−18	1.10E−18	1.6E−19	1.29E−17	1.8E−18	2.39E−19	3.4E−20

Table 2. (Continued.)

θ (deg)	Sum	Error	$3p^5 4s[3/2]^o_2$	Error	$3p^5 4s[3/2]^o_1$	Error	$3p^5 4s'[1/2]^o_0$	Error
15	2.91E−17	3.9E−18	1.05E−18	1.4E−19	6.36E−18	8.6E−19	2.42E−19	3.3E−20
20	1.29E−17	1.6E−18	9.39E−19	1.2E−19	2.82E−18	3.5E−19	1.87E−19	2.4E−20
25	7.36E−18	9.2E−19	8.49E−19	1.1E−19	1.65E−18	2.1E−19	1.75E−19	2.2E−20
30	5.16E−18	6.6E−19	7.58E−19	9.7E−20	1.15E−18	1.5E−19	1.53E−19	2.0E−20
35	3.95E−18	5.1E−19	6.13E−19	8.0E−20	8.89E−19	1.1E−19	1.23E−19	1.6E−20
40	2.75E−18	3.5E−19	4.26E−19	5.5E−20	6.20E−19	8.0E−20	8.44E−20	1.1E−20
45	2.12E−18	2.8E−19	2.95E−19	4.0E−20	4.74E−19	6.3E−20	5.81E−20	8.1E−21
50	1.47E−18	2.0E−19	1.89E−19	2.6E−20	3.20E−19	4.3E−20	3.52E−20	4.9E−21
55	1.18E−18	1.6E−19	1.09E−19	1.5E−20	2.62E−19	3.6E−20	2.14E−20	3.1E−21
60	7.87E−19	9.9E−20	4.99E−20	6.8E−21	1.67E−19	2.2E−20	9.40E−21	1.5E−21
65	5.54E−19	6.9E−20	2.03E−20	3.1E−21	1.14E−19	1.5E−20	2.41E−21	7.8E−22
70	4.88E−19	6.1E−20	1.35E−20	2.1E−21	1.02E−19	1.3E−20	1.99E−21	6.1E−22
75	4.53E−19	5.7E−20	1.89E−20	2.7E−21	9.48E−20	1.2E−20	4.14E−21	7.7E−22
80	4.13E−19	5.2E−20	2.25E−20	3.1E−21	8.90E−20	1.2E−20	4.56E−21	7.8E−22
85	4.16E−19	5.2E−20	2.97E−20	4.4E−21	9.22E−20	1.3E−20	4.92E−21	1.1E−21
90	4.20E−19	5.2E−20	3.74E−20	5.1E−21	9.09E−20	1.2E−20	7.16E−21	1.2E−21
95	4.19E−19	5.3E−20	4.08E−20	5.9E−21	9.22E−20	1.3E−20	6.43E−21	1.3E−21
100	4.19E−19	5.4E−20	4.70E−20	6.7E−21	9.37E−20	1.3E−20	7.97E−21	1.4E−21
105	4.18E−19	5.4E−20	5.45E−20	7.9E−21	9.30E−20	1.3E−20	1.08E−20	1.9E−21
110	4.16E−19	5.3E−20	5.41E−20	7.7E−21	9.35E−20	1.3E−20	1.07E−20	1.8E−21
115	4.19E−19	5.4E−20	5.68E−20	8.4E−21	9.73E−20	1.4E−20	9.98E−21	1.9E−21
120	4.21E−19	5.4E−20	5.65E−20	7.4E−21	9.46E−20	1.2E−20	1.07E−20	1.5E−21
125	4.26E−19	5.5E−20	6.25E−20	8.4E−21	9.70E−20	1.3E−20	1.25E−20	1.8E−21
130	4.30E−19	5.7E−20	7.59E−20	1.0E−20	9.80E−20	1.3E−20	1.69E−20	2.4E−21

θ (deg)	$3p^5 4s'[1/2]^o_1$	Error	r	Error	r'	Error	r''	Error
3			4.68E+00	3.1E−01	2.87E−01	6.3E−05	4.75E−02	1.1E−03
5	8.36E−17	1.2E−17	4.45E+00	2.1E−01	2.89E−01	4.8E−06	5.18E−02	9.7E−04
8			4.63E+00	2.3E−01	2.84E−01	7.8E−06	6.86E−02	1.3E−03
10	4.46E−17	6.3E−18	4.62E+00	1.8E−01	2.88E−01	5.2E−06	8.57E−02	1.4E−03
15	2.14E−17	2.9E−18	4.35E+00	1.7E−01	2.97E−01	9.5E−06	1.66E−01	2.7E−03
20	8.94E−18	1.1E−18	5.02E+00	1.5E−01	3.15E−01	4.6E−05	3.33E−01	3.7E−03
25	4.69E−18	5.9E−19	4.82E+00	1.7E−01	3.52E−01	2.0E−04	5.13E−01	7.2E−03
30	3.09E−18	4.0E−19	4.97E+00	1.6E−01	3.72E−01	2.1E−03	6.59E−01	9.6E−03
35	2.33E−18	3.0E−19	4.97E+00	1.7E−01	3.82E−01	2.6E−04	6.89E−01	9.3E−03
40	1.62E−18	2.1E−19	5.01E+00	2.3E−01	3.83E−01	4.9E−04	6.82E−01	1.2E−02
45	1.29E−18	1.7E−19	5.08E+00	2.4E−01	3.67E−01	3.2E−04	6.22E−01	1.2E−02
50	9.28E−19	1.3E−19	5.35E+00	3.3E−01	3.45E−01	5.3E−04	5.89E−01	1.4E−02
55	7.92E−19	1.1E−19	5.14E+00	4.5E−01	3.31E−01	4.3E−04	4.17E−01	1.4E−02
60	5.60E−19	7.3E−20	5.31E+00	5.4E−01	2.99E−01	8.6E−05	2.98E−01	1.1E−02
65	4.17E−19	5.5E−20	8.44E+00	2.6E+00	2.74E−01	3.2E−04	1.78E−01	1.3E−02
70	3.71E−19	4.9E−20	6.79E+00	2.0E+00	2.74E−01	3.6E−03	1.33E−01	1.0E−02
75	3.35E−19	4.4E−20	4.67E+00	9.8E−01	2.83E−01	6.2E−03	2.00E−01	1.6E−02
80	2.97E−19	3.8E−20	4.89E+00	8.2E−01	3.00E−01	5.1E−03	2.52E−01	1.6E−02
85	2.89E−19	3.9E−20	6.03E+00	1.1E+00	3.19E−01	1.0E−02	3.22E−01	2.2E−02
90	2.84E−19	3.7E−20	5.07E+00	8.3E−01	3.21E−01	9.4E−03	4.04E−01	2.6E−02
95	2.80E−19	3.8E−20	6.34E+00	9.4E−01	3.29E−01	1.0E−02	4.42E−01	2.5E−02
100	2.70E−19	3.7E−20	5.90E+00	6.7E−01	3.47E−01	4.3E−04	5.02E−01	2.0E−02
105	2.59E−19	3.6E−20	5.05E+00	5.6E−01	3.58E−01	1.1E−02	5.86E−01	3.1E−02
110	2.58E−19	3.5E−20	5.07E+00	5.1E−01	3.62E−01	1.0E−02	5.79E−01	2.8E−02

Table 2. (Continued.)

θ (deg)	$3p^5 4s'[1/2]^o_1$	Error	r	Error	r'	Error	r''	Error
115	2.55E−19	3.6E−20	5.69E+00	7.5E−01	3.82E−01	1.3E−02	5.84E−01	3.4E−02
120	2.59E−19	3.4E−20	5.28E+00	6.7E−01	3.68E−01	1.2E−02	5.95E−01	3.3E−02
125	2.53E−19	3.4E−20	5.03E+00	6.2E−01	3.85E−01	1.0E−02	6.41E−01	3.4E−02
130	2.39E−19	3.2E−20	4.48E+00	4.4E−01	4.16E−01	1.2E−02	7.64E−01	3.7E−02

(f) 50 eV argon

θ (deg)	Sum	Error	$3p^5 4s[3/2]^o_2$	Error	$3p^5 4s[3/2]^o_1$	Error	$3p^5 4s'[1/2]^o_0$	Error
0								
1								
3								
4								
5	1.55E−16	2.6E−17	6.29E−20	1.2E−20	3.28E−17	5.6E−18	6.40E−20	1.2E−20
8								
10	5.10E−17	8.7E−18	6.08E−20	1.1E−20	1.07E−17	1.8E−18	2.50E−20	4.8E−21
15	1.67E−17	2.8E−18	9.35E−20	1.7E−20	3.48E−18	6.0E−19	2.42E−20	4.9E−21
20	6.31E−18	1.1E−18	9.62E−20	1.7E−20	1.31E−18	2.2E−19	1.79E−20	3.2E−21
25	3.47E−18	5.9E−19	9.60E−20	1.7E−20	7.29E−19	1.2E−19	1.91E−20	3.4E−21
30	2.46E−18	4.2E−19	8.68E−20	1.5E−20	5.17E−19	8.9E−20	2.18E−20	3.8E−21
35	2.13E−18	3.7E−19	7.73E−20	1.4E−20	4.50E−19	7.8E−20	2.11E−20	3.9E−21
40	1.57E−18	2.7E−19	5.47E−20	9.7E−21	3.26E−19	5.7E−20	1.19E−20	2.2E−21
45	1.19E−18	2.0E−19	4.34E−20	7.9E−21	2.52E−19	4.4E−20	7.85E−21	1.8E−21
50	8.10E−19	1.4E−19	3.08E−20	5.3E−21	1.68E−19	2.9E−20	7.16E−21	1.3E−21
55	5.33E−19	9.0E−20	1.97E−20	3.4E−21	1.14E−19	2.0E−20	5.06E−21	9.6E−22
60	3.02E−19	5.1E−20	1.27E−20	2.2E−21	6.56E−20	1.1E−20	2.01E−21	4.1E−22
65	2.03E−19	3.5E−20	9.77E−21	1.7E−21	4.31E−20	7.5E−21	2.38E−21	4.8E−22
70	1.65E−19	2.8E−20	8.12E−21	1.5E−21	3.40E−20	6.0E−21	2.03E−21	4.4E−22
75	1.94E−19	3.3E−20	1.09E−20	2.0E−21	3.98E−20	7.1E−21	3.57E−21	7.5E−22
80	2.34E−19	4.1E−20	1.08E−20	1.9E−21	5.03E−20	8.9E−21	2.67E−21	5.5E−22
85	3.87E−19	6.7E−20	1.47E−20	2.8E−21	7.95E−20	1.4E−20	3.73E−21	8.7E−22
90	4.19E−19	7.2E−20	1.41E−20	2.5E−21	8.53E−20	1.5E−20	3.77E−21	7.7E−22
95	4.60E−19	8.2E−20	1.39E−20	2.6E−21	9.58E−20	1.7E−20	3.89E−21	8.4E−22
100	5.29E−19	9.5E−20	1.73E−20	3.2E−21	1.15E−19	2.1E−20	4.05E−21	8.5E−22
105	3.44E−19	6.2E−20	1.22E−20	2.3E−21	7.43E−20	1.4E−20	3.76E−21	7.9E−22
110	3.02E−19	5.5E−20	1.32E−20	2.4E−21	6.37E−20	1.2E−20	3.13E−21	6.2E−22
115	3.46E−19	6.4E−20	1.65E−20	3.1E−21	7.32E−20	1.4E−20	4.32E−21	8.9E−22
120	2.51E−19	4.7E−20	1.45E−20	2.8E−21	5.27E−20	1.0E−20	3.41E−21	7.1E−22
125	2.00E−19	3.8E−20	1.41E−20	2.8E−21	4.30E−20	8.2E−21	3.59E−21	7.7E−22
130	1.69E−19	3.3E−20	1.61E−20	3.2E−21	3.71E−20	7.4E−21	2.71E−21	6.0E−22

θ (deg)	$3p^5 4s'[1/2]^o_1$	Error	r	Error	r'	Error	r''	Error
0			1.49E+00	3.5E−01	2.80E−01	6.0E−04	3.17E−03	4.5E−04
1			6.74E−01	1.9E−01	2.78E−01	2.4E−05	1.91E−03	4.3E−04
3			2.14E+00	2.5E+00	2.72E−01	2.9E−05	1.03E−03	7.0E−04
4			4.87E−01	2.4E−01	2.74E−01	1.1E−06	7.24E−04	3.2E−04
5	1.22E−16	2.1E−17	1.02E+00	2.5E−01	2.70E−01	3.0E−06	1.82E−03	3.0E−04
8			1.35E+00	4.7E−01	2.66E−01	2.5E−06	2.59E−03	6.0E−04
10	4.01E−17	6.8E−18	2.39E+00	4.2E−01	2.68E−01	4.2E−06	5.63E−03	5.2E−04
15	1.31E−17	2.2E−18	3.86E+00	4.5E−01	2.66E−01	1.8E−06	2.68E−02	1.3E−03
20	4.89E−18	8.4E−19	7.11E+00	2.0E+00	2.69E−01	9.4E−05	7.26E−02	3.6E−03
25	2.63E−18	4.5E−19	4.95E+00	4.2E−01	2.78E−01	3.9E−05	1.35E−01	4.4E−03

Table 2. (Continued.)

θ (deg)	$3p^5 4s'[1/2]^o_1$	Error	r	Error	r'	Error	r''	Error
30	1.83E−18	3.2E−19	4.03E+00	3.1E−01	2.82E−01	7.0E−04	1.69E−01	5.3E−03
35	1.58E−18	2.7E−19	3.90E+00	4.1E−01	2.85E−01	1.8E−03	1.70E−01	6.9E−03
40	1.17E−18	2.1E−19	4.60E+00	4.7E−01	2.78E−01	4.7E−04	1.66E−01	6.8E−03
45	8.82E−19	1.5E−19	5.52E+00	9.2E−01	2.86E−01	2.9E−03	1.72E−01	1.0E−02
50	6.04E−19	1.0E−19	4.79E+00	6.8E−01	2.76E−01	5.7E−04	1.81E−01	9.0E−03
55	3.93E−19	6.7E−20	4.31E+00	8.0E−01	2.83E−01	6.6E−03	1.70E−01	1.2E−02
60	2.21E−19	3.8E−20	8.46E+00	5.5E+00	3.05E−01	4.0E−03	1.85E−01	5.5E−02
65	1.48E−19	2.6E−20	5.28E+00	2.6E+00	2.97E−01	8.9E−03	2.21E−01	2.3E−02
70	1.21E−19	2.1E−20	4.12E+00	1.4E+00	2.82E−01	1.4E−02	2.47E−01	3.0E−02
75	1.40E−19	2.5E−20	3.09E+00	8.4E−01	2.90E−01	1.3E−02	2.60E−01	3.0E−02
80	1.70E−19	3.0E−20	5.49E+00	3.0E+00	3.07E−01	1.1E−02	2.02E−01	2.4E−02
85	2.89E−19	5.1E−20	6.85E+00	5.5E+00	2.85E−01	1.2E−02	1.77E−01	2.2E−02
90	3.15E−19	5.5E−20	4.80E+00	1.5E+00	2.71E−01	4.6E−03	1.66E−01	1.3E−02
95	3.46E−19	6.3E−20	3.83E+00	1.3E+00	2.76E−01	6.5E−03	1.53E−01	1.7E−02
100	3.93E−19	7.1E−20	4.16E+00	1.1E+00	2.88E−01	4.1E−03	1.48E−01	1.4E−02
105	2.53E−19	4.6E−20	3.43E+00	6.8E−01	2.92E−01	3.0E−03	1.61E−01	1.3E−02
110	2.21E−19	4.0E−20	4.67E+00	1.1E+00	2.88E−01	6.5E−03	2.07E−01	1.5E−02
115	2.52E−19	4.7E−20	4.48E+00	1.1E+00	2.88E−01	4.6E−03	2.22E−01	1.6E−02
120	1.80E−19	3.4E−20	5.34E+00	1.5E+00	2.94E−01	9.3E−03	2.67E−01	2.0E−02
125	1.39E−19	2.7E−20	5.13E+00	1.5E+00	3.05E−01	8.7E−03	3.30E−01	2.7E−02
130	1.13E−19	2.3E−20	6.18E+00	1.7E+00	3.27E−01	1.2E−02	4.52E−01	3.8E−02

(g) 100 eV argon

θ (deg)	Sum	Error	$3p^5 4s[3/2]^o_2$	Error	$3p^5 4s[3/2]^o_1$	Error	$3p^5 4s'[1/2]^o_0$	Error
5	2.79E−16	4.8E−17	7.96E−20	1.8E−20	5.82E−17	1.0E−17	6.94E−20	1.7E−20
10	2.05E−17	3.6E−18	2.49E−20	4.7E−21	4.25E−18	7.4E−19	6.21E−21	1.6E−21
15	5.88E−18	1.0E−18	4.04E−20	7.4E−21	1.19E−18	2.1E−19	9.57E−21	2.1E−21
20	1.66E−18	2.9E−19	2.57E−20	4.7E−21	3.40E−19	5.9E−20	5.68E−21	1.2E−21
25	1.15E−18	2.0E−19	1.13E−20	2.2E−21	2.35E−19	4.1E−20	2.64E−21	7.2E−22
30	8.50E−19	1.5E−19	4.42E−21	8.7E−22	1.73E−19	3.0E−20	1.77E−21	4.3E−22
35	5.50E−19	9.5E−20	1.82E−21	4.7E−22	1.12E−19	2.0E−20	5.45E−22	2.7E−22
40	3.37E−19	5.8E−20	2.85E−21	8.5E−22	6.33E−20	1.1E−20	1.35E−21	6.0E−22
45	1.86E−19	3.2E−20	3.26E−21	9.2E−22	3.51E−20	6.7E−21	1.68E−21	7.0E−22
50	1.08E−19	1.9E−20	1.82E−21	3.7E−22	2.23E−20	4.0E−21	3.95E−22	1.4E−22
55	7.10E−20	1.2E−20	1.25E−21	3.4E−22	1.47E−20	2.9E−21	1.36E−22	1.7E−22
60	4.79E−20	8.4E−21	1.42E−21	3.5E−22	1.00E−20	2.0E−21	3.24E−22	1.5E−22
65	4.29E−20	7.6E−21	9.47E−22	3.2E−22	8.85E−21	1.9E−21	3.39E−22	2.6E−22
70	4.92E−20	8.7E−21	9.55E−22	2.2E−22	1.02E−20	1.9E−21	3.55E−22	1.2E−22
75	5.97E−20	1.0E−20	5.32E−22	3.5E−22	1.15E−20	2.3E−21	2.35E−22	2.8E−22
80	7.56E−20	1.3E−20	9.45E−22	1.9E−22	1.56E−20	2.7E−21	1.77E−22	5.7E−23
85	9.18E−20	1.6E−20	1.41E−21	3.4E−22	1.79E−20	3.3E−21	2.36E−22	1.6E−22
90	9.29E−20	1.6E−20	1.74E−21	3.9E−22	1.90E−20	3.5E−21	2.74E−22	1.6E−22
95	9.28E−20	1.6E−20	3.78E−21	2.0E−21	1.46E−20	4.5E−21	1.70E−21	1.8E−21
100	8.51E−20	1.5E−20	2.18E−21	4.6E−22	1.67E−20	3.1E−21	3.85E−22	1.6E−22
105	7.57E−20	1.3E−20	2.24E−21	4.8E−22	1.65E−20	3.1E−21	3.42E−22	1.6E−22
110	5.09E−20	8.8E−21	2.45E−21	5.1E−22	1.08E−20	2.0E−21	4.70E−22	1.6E−22
115	3.64E−20	6.5E−21	3.05E−21	6.8E−22	7.67E−21	1.5E−21	5.44E−22	2.0E−22
120	2.50E−20	4.6E−21	3.22E−21	6.3E−22	5.53E−21	1.1E−21	6.05E−22	1.5E−22
125	1.07E−20	1.9E−21	2.35E−21	4.9E−22	2.38E−21	4.8E−22	5.04E−22	1.3E−22
130	1.05E−20	1.88E−21	1.47E−21	2.9E−22	2.30E−21	4.4E−22	2.52E−22	6.5E−23

Table 2. (Continued.)

θ (deg)	$3p^5 4s'[1/2]^o_1$	Error	r	Error	r'	Error	r''	Error
5	2.21E−16	3.8E−17	1.15E+00	3.8E−01	2.63E−01	1.4E−03	2.85E−01	3.9E−04
10	1.62E−17	2.8E−18	4.01E+00	1.3E+00	2.62E−01	5.9E−03	2.56E−01	1.5E−03
15	4.64E−18	8.1E−19	4.22E+00	1.2E+00	2.57E−01	3.4E−02	2.54E−01	8.6E−03
20	1.29E−18	2.2E−19	4.53E+00	1.3E+00	2.64E−01	7.6E−02	2.52E−01	1.9E−02
25	9.02E−19	1.6E−19	4.29E+00	1.4E+00	2.60E−01	4.8E−02	2.60E−01	1.3E−02
30	6.70E−19	1.2E−19	2.49E+00	7.8E−01	2.59E−01	2.5E−02	2.63E−01	6.7E−03
35	4.36E−19	7.6E−20	3.33E+00	1.9E+00	2.57E−01	1.6E−02	3.13E−01	5.1E−03
40	2.69E−19	4.8E−20	2.11E+00	1.1E+00	2.36E−01	4.5E−02	3.47E−01	1.6E−02
45	1.45E−19	2.7E−20	1.95E+00	9.8E−01	2.41E−01	9.3E−02	3.42E−01	3.2E−02
50	8.33E−20	1.5E−20	4.60E+00	1.8E+00	2.68E−01	8.1E−02	2.71E−01	2.2E−02
55	5.49E−20	1.0E−20	9.19E+00	1.2E+01	2.68E−01	8.5E−02	3.34E−01	2.8E−02
60	3.61E−20	7.0E−21	4.38E+00	2.3E+00	2.78E−01	1.4E−01	3.18E−01	4.5E−02
65	3.29E−20	6.7E−21	2.79E+00	2.3E+00	2.69E−01	1.1E−01	3.95E−01	4.2E−02
70	3.77E−20	6.8E−21	2.69E+00	1.1E+00	2.71E−01	9.4E−02	2.91E−01	2.7E−02
75	4.68E−20	9.1E−21	2.26E+00	3.1E+00	2.46E−01	4.6E−02	6.79E−01	3.1E−02
80	5.88E−20	1.0E−20	5.35E+00	2.0E+00	2.65E−01	6.1E−02	2.64E−01	1.6E−02
85	7.22E−20	1.3E−20	5.98E+00	4.3E+00	2.48E−01	7.9E−02	3.02E−01	2.4E−02
90	7.17E−20	1.3E−20	6.34E+00	4.0E+00	2.66E−01	9.1E−02	2.88E−01	2.6E−02
95	7.27E−20	1.9E−20	2.23E+00	2.6E+00	2.01E−01	2.6E−01	6.19E−01	1.6E−01
100	6.57E−20	1.2E−20	5.66E+00	2.6E+00	2.55E−01	1.3E−01	2.79E−01	3.6E−02
105	5.66E−20	1.0E−20	6.55E+00	3.4E+00	2.91E−01	1.4E−01	2.86E−01	3.9E−02
110	3.67E−20	6.7E−21	5.21E+00	2.0E+00	2.93E−01	2.3E−01	2.78E−01	6.3E−02
115	2.49E−20	4.9E−21	5.62E+00	2.4E+00	3.09E−01	4.0E−01	2.97E−01	1.2E−01
120	1.53E−20	2.9E−21	5.31E+00	1.7E+00	3.61E−01	5.8E−01	2.75E−01	1.6E−01
125	5.15E−21	1.1E−21	4.65E+00	1.5E+00	4.61E−01	9.9E−01	2.88E−01	2.8E−01
130	6.45E−21	1.2E−21	5.83E+00	1.9E+00	3.56E−01	6.4E−01	2.75E−01	1.8E−01

different double-minimum shape of the DCSs from experiment at 15 eV as compared to the single-minimum shape of the DCSs at 14 eV. The UFOMBT and the RM41 show shapes similar to that of experiment, but the shapes of RM5 and RM5a (which are indistinguishable here) and the DWBA and SCGS shapes remain similar to the single minimum shape observed at 14 eV.

At $E_0 = 17.5$ eV, figure 2(c), the situation between theory and experiment remains similar to that for $E_0 = 15$ eV. We note the increased double-minimum shape in the experimental results, which is more closely reproduced by the UFOMBT.

At $E_0 = 20$ eV, figure 2(d), the strong double-minimum shape of the DCSs is reduced and we have now two other measurements with which to compare. These are the DCSs of Filipovic *et al* (2000a, 2000b) and Chutjian and Cartwright (1981). Clearly, agreement of the present experimental DCSs with the DCSs of Filipovic *et al* (2000a, 2000b) is excellent (except at large $\theta > 110°$), and significantly better than with those of Chutjian and Cartwright (1981). Agreement with the RM5 and RM5a (again indistinguishable) is much improved, but significant deviations are observed for $\theta > 90°$. The other calculations either give poor shapes, or magnitudes or both. Confirmation of our results with those of Filipovic *et al* (2000a, 2000b) is encouraging.

At $E_0 = 30$ eV, figure 2(e), agreement between the present experiment and the measurements of Chutjian and Cartwright (1981) is very good except at $\theta < 40°$. At around $\theta = 70°$, the elastic scattering DCSs for Ar show a steep minimum, with a narrow width of about 6°. As previously discussed, normalization to this DCS is very sensitive to the placement of the analyser and results (after averaging) in a dispersion profile as shown in the figure. To

Table 3. Summary of 1 standard deviation experimental uncertainties in percentages. See the text for a further discussion.

Energy (eV)	Absolute standard DCSs Ar	Relative transmission inelastic	Transmission elastic to inelastic	Statistical uncertainty $3p^5 4s$	Statistical uncertainty and unfolding $3p^5 4s[3/2]^o_2$	Statistical uncertainty and unfolding $3p^5 4s[3/2]^o_1$	Statistical uncertainty and unfolding $3p^5 4s'[1/2]^o_0$		
14	8	5	8	4.6	8.8	8.3	18.7		
15	7	4.5	8	2.7	5.1	4.6	11.9		
17.5	8	4	7.5	1.5	2.8	2.8	5.9		
20	8	3	6	1.8	3.5	3.3	5.6		
30	15	2	5	1.8	4.0	3.2	7.4		
50	13.5	1	4	1.5	4.6	2.4	9.9		
100	13.5	1	3	4.0	13.5	6.3	36.0		
Energy (eV)	Statistical uncertainty and unfolding $3p^5 4s'[1/2]^o_1$	Error summed DCS $3p^5 4s$	Overall error DCS $3p^5 4s[3/2]^o_2$	Overall error DCS $3p^5 4s[3/2]^o_1$	Overall error DCS $3p^5 4s'[1/2]^o_0$	Overall error DCS $3p^5 4s'[1/2]^o_1$	Overall error r	Overall error r'	Overall error r''
14	7.5	12.2	14.3	14.0	21.9	13.6	21.3	12.3	13.1
15	4.6	11.0	11.8	11.6	16.0	11.6	13.7	7.9	8.2
17.5	2.5	11.1	11.3	11.3	12.5	11.2	7.7	5.5	5.6
20	3.0	10.2	10.6	10.5	11.5	10.4	7.3	5.4	5.7
30	2.9	15.9	16.3	16.1	17.5	16.1	8.6	4.8	5.5
50	2.3	14.2	14.8	14.3	17.2	14.3	11.0	3.5	5.3
100	5.6	14.4	19.3	15.2	38.6	14.9	38.5	8.5	14.9

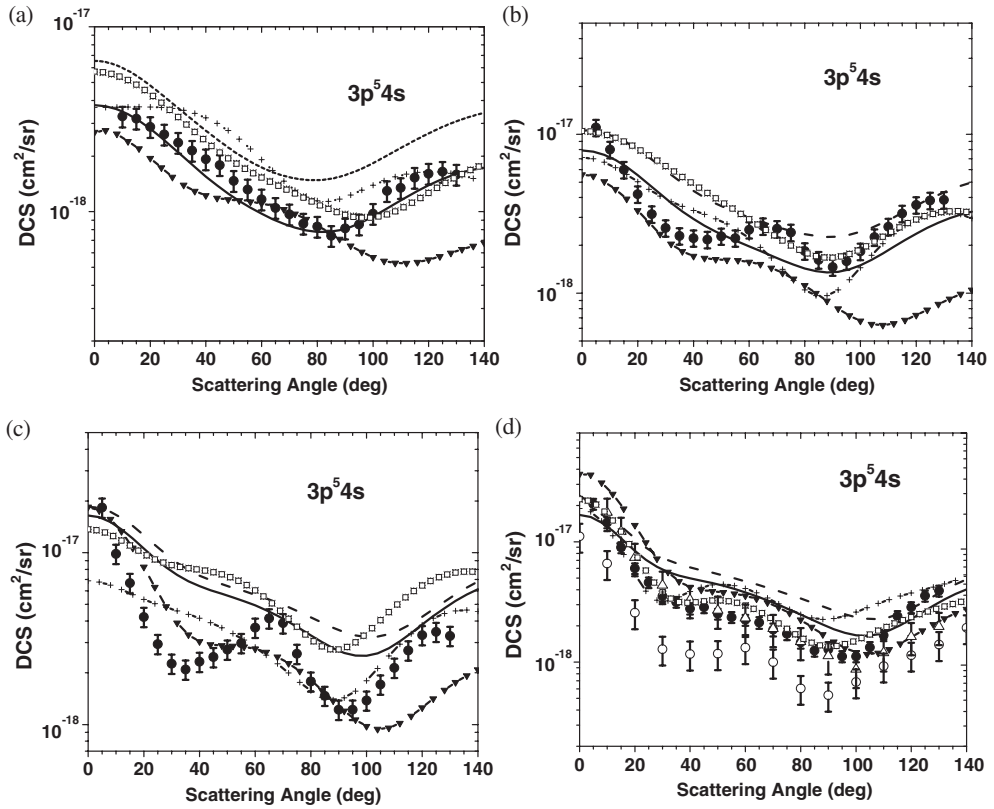

Figure 2. DCSs for the electron impact excitation of the summed $3p^5 4s$ feature in Ar. Experiments: ●, present data; △, Filipovic *et al* (2000a, 2000b); ○, Chutjian and Cartwright (1981); ◇, Khakoo *et al* (1994). Theories: ——, SCGS-RDWA; — — —, DWBA; —▼—, Single configuration UFOMBT; — + —, 41-state *R*-matrix (RM41); _⋇_, 5-state *R*-matrix (RM5); —□—, 5-state *R*-matrix using the CIV3-5 code, but with adjusted intermediate-coupling coefficients (RM5a). (a) $E_0 = 14$ eV, (b) $E_0 = 15$ eV, (c) $E_0 = 17.5$ eV, (d) $E_0 = 20$ eV, (e) $E_0 = 30$ eV with the dash-star line (_☆_) representing DCSs obtained entirely by, and showing the effect of, normalizing to the elastic DCS around the minimum (see the text for details), (f) $E_0 = 50$ eV and (g) $E_0 = 100$ eV. See also tables 2(a)–(g) and the text for a further discussion.

make a more reliable measurement, we applied the method of mixtures with Ne (Khakoo *et al* 2002) and used the $E_0 = 30$ eV DCSs for the excitation of the Ne $2p^5 3s$ configuration from Khakoo *et al* (2002). This results in the corrected smoother DCS profile shown. However, the method of mixtures could not be applied throughout all these measurements because the excitation energy of the Ne $2p^5 3s$ configuration is high (≈16.8 eV). This method could therefore only be accurately implemented at E_0 values above ≈19 eV where the Ne DCSs are large. Agreement between the present measurements and those of Chutjian and Cartwright (1981) is very good at large angles except around $\theta = 70°$ where the problems in normalizing to the elastic DCS is prevalent and would certainly have affected their measurements as well. Also shown are earlier measurements taken by our group, which show good agreement with Chutjian and Cartwright (1981). Agreement between experiment and theory is much improved compared to 20 eV. We see most of the theories agreeing very well in shape, although the overall theoretical picture is still not completely satisfactory.

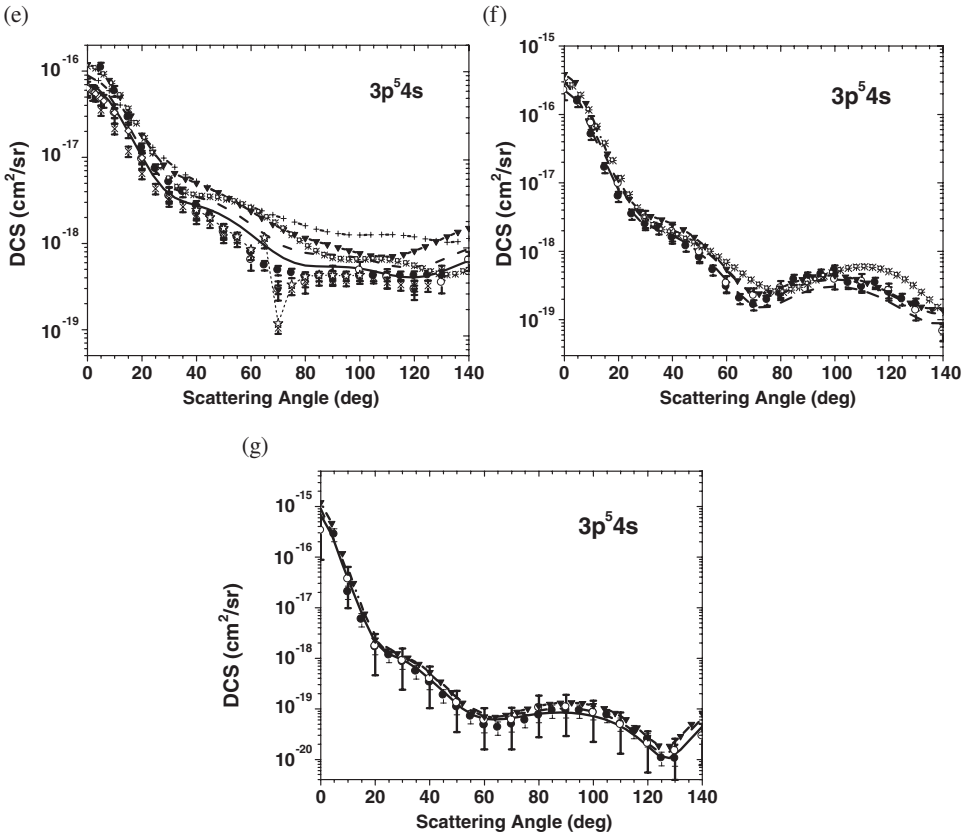

Figure 2. (Continued.)

At $E_0 = 50$ eV, figure 2(f), agreement between the experimental measurements is excellent at all θ values. Agreement between the present experiment and theory is also very good. The best agreement is observed with the SCGS-RDWA calculations, followed by the DWBA and UFOMBT, which are slightly higher in magnitude. The *R*-matrix theory would rarely be applied at this energy; nevertheless, the RM5 and RM5a models, which maintain the tight coupling between the ground state and the $3p^5 4s$ configuration, perform sufficiently well, and better than the 41-state *R*-matrix expansion. In contrast to other situations, particularly in atomic structure calculations, we note that there is no formal guarantee for improvement of close-coupling results by simply increasing the number of states until ultimate convergence (an almost unrealistic goal in the present situation) is reached.

At $E_0 = 100$ eV, figure 2(g), only perturbative theories are shown. All of these do excellently. However, the SCGS-RDWA does slightly better than the UFOMBT and the DWBA. The agreement between the experiments is very good except that the $\theta = 0°$ DCS of Chutjian and Cartwright is significantly lower than the closely-spaced theories, whereas our smallest θ DCS at 5° remains in very good agreement with theory. Improvements in the summed DCSs from the UFOMBT and DWBA were only achieved when their (α, β) mixing coefficients were adjusted to those from OOS measurements (Chan *et al* 1992).

We also note here that the DWBA and SCGS-RDWA show similar overall angular distributions, but disagree quantitatively in increasing amounts at lower E_0 values.

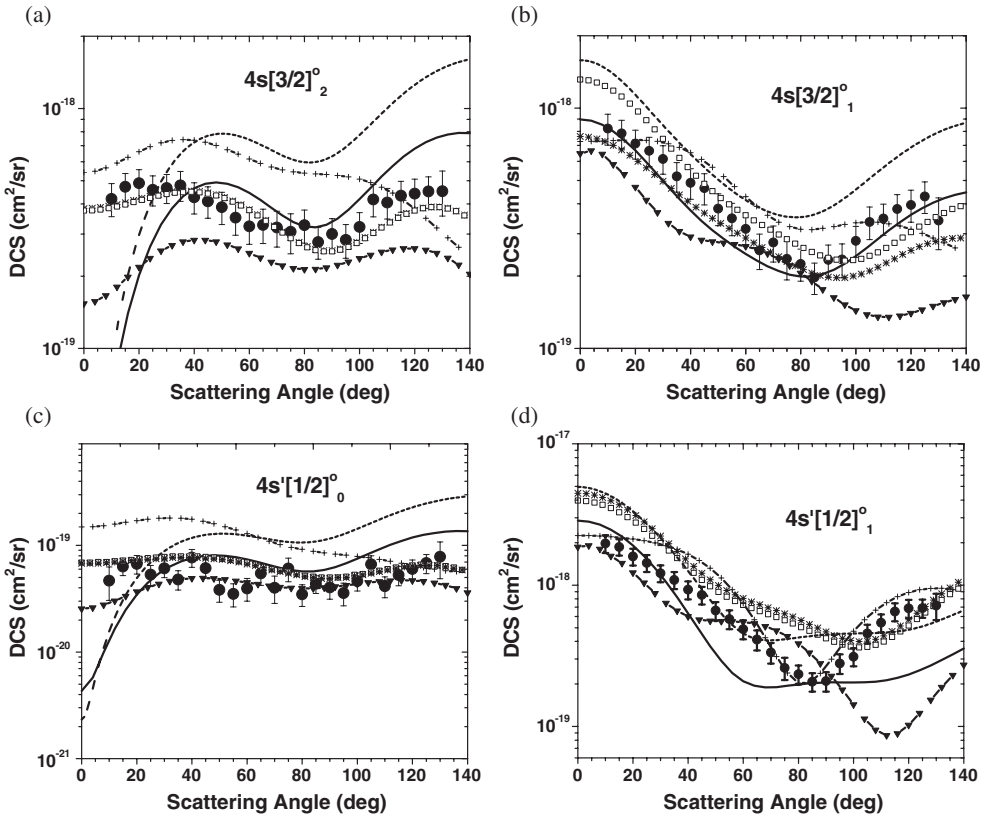

Figure 3. DCSs for the electron impact excitation of the individual levels comprising the $3p^5 4s$ configuration of Ar at $E_0 = 14$ eV. See also table 2. The legend is the same as in figure 2. (a) $(3p^5 4s)[3/2]^o_2$ feature, (b) $(3p^5 4s)[3/2]^o_1$ feature, (c) $(3p^5 4s')[1/2]^o_0$ feature and (d) $(3p^5 4s')[1/2]^o_1$ feature. For the metastable levels ($J = 2, 0$, figures (a) and (c)) the RM5a theory is not plotted, since it essentially equals RM5 for this feature. See the text for further discussion.

3.2. Individual level DCSs

Our $E_0 = 15$ eV data are left out of the following discussion because they show similar behaviour to our results at $E_0 = 17.5$ eV. The RM5 and RM5a calculations for the metastable states are nearly identical. The reason for the small differences is the fact that changing the intermediate coupling coefficients changes the channel coupling slightly, and thus produces an indirect effect also on these metastable states. Consequently for the metastable levels' DCSs and the ratio r which concerns these DCSs, only the RM5 will be discussed and plotted in the corresponding graphs. In these cases we refer to both as RM5/a.

Figures 3(a)–(d) show the DCSs at $E_0 = 14$ eV. Clearly the RM5/a gives very good agreement with the experimental DCSs for the triplet metastable levels, but for the singlet dipole-allowed transition the agreement is qualitative. The SCGS gives very good agreement for the $(3p^5 4s)[3/2]^o_1$ level, but gives poor agreement for the $(3p^5 4s')[1/2]^o_1$ level. For the $(3p^5 4s')[1/2]^o_1$ level the RM5a is about 10% lower than the RM5 at all angles, while for the $(3p^5 4s)[3/2]^o_1$ level the RM5 calculation is a factor of 1.3–2 higher over the angular range. Clearly none of the perturbative methods is applicable in this energy range.

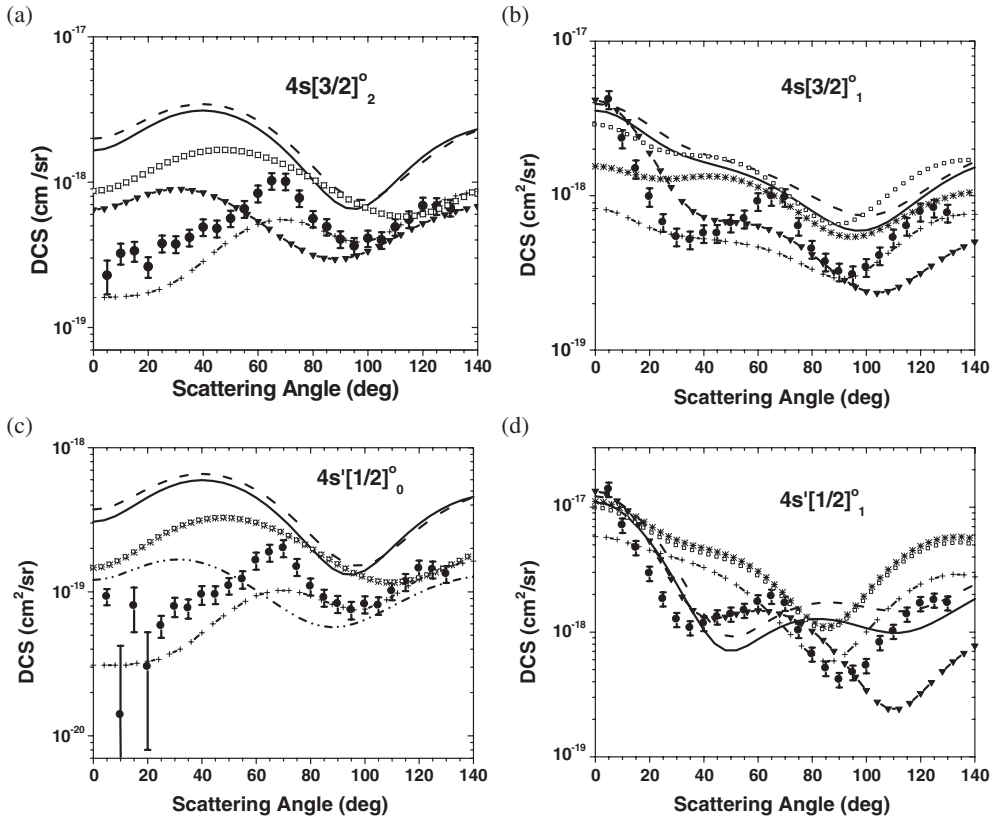

Figure 4. The same as figure 3, but for $E_0 = 17.5$ eV.

Figures 4(a)–(d) show the DCSs at $E_0 = 17.5$ eV. Here, for the two metastable levels, qualitative agreement with the RM41 data is observed, but for the optically allowed transitions these DCSs are not in good agreement. The experimental DCSs for these transitions display a very strong double-minimum, which is not predicted by any of the models.

Figures 5(a)–(d) show the individual level DCSs at 20 eV. For the $(3p^5 4s)[3/2]^o_2$ level, the RM5/a do the best of all the models, but above $\theta = 110°$ (see figure 5(a)), these models diverge rapidly from the experimental DCSs. Similar behaviour is observed for the RM5/a results for the $(3p^5 4s')[1/2]^o_0$ level in figure 5(c). For the $(3p^5 4s)[3/2]^o_1$ level the RM5a shows a significant improvement over the RM5 and demonstrates the importance of using the correct mixing coefficients. The perturbative models display somewhat good agreement for the $(3p^5 4s')[1/2]^o_1$ DCS (figure 5(d)) at small θ, but show unsatisfactory comparisons at generally larger θ. Agreement between the present measurements and the experimental DCSs of Filipovic *et al* (2000a, 2000b) is very good. However, significant disagreements with the results of Chutjian and Cartwright (1981) are observed.

Figures 6(a)–(d) show the individual DCSs at $E_0 = 30$ eV, but here, unlike at $E_0 = 20$ eV, a significant improvement in agreement with the results of Chutjian and Cartwright (1981) is observed. Of the models, the best agreement is provided by the SCGS-RDWA for the dipole-allowed levels. Otherwise, the RM5/a do surprisingly well. The other perturbative models show improvements, as compared to $E_0 = 20$ eV. Nevertheless, the overall situation still requires considerable improvement.

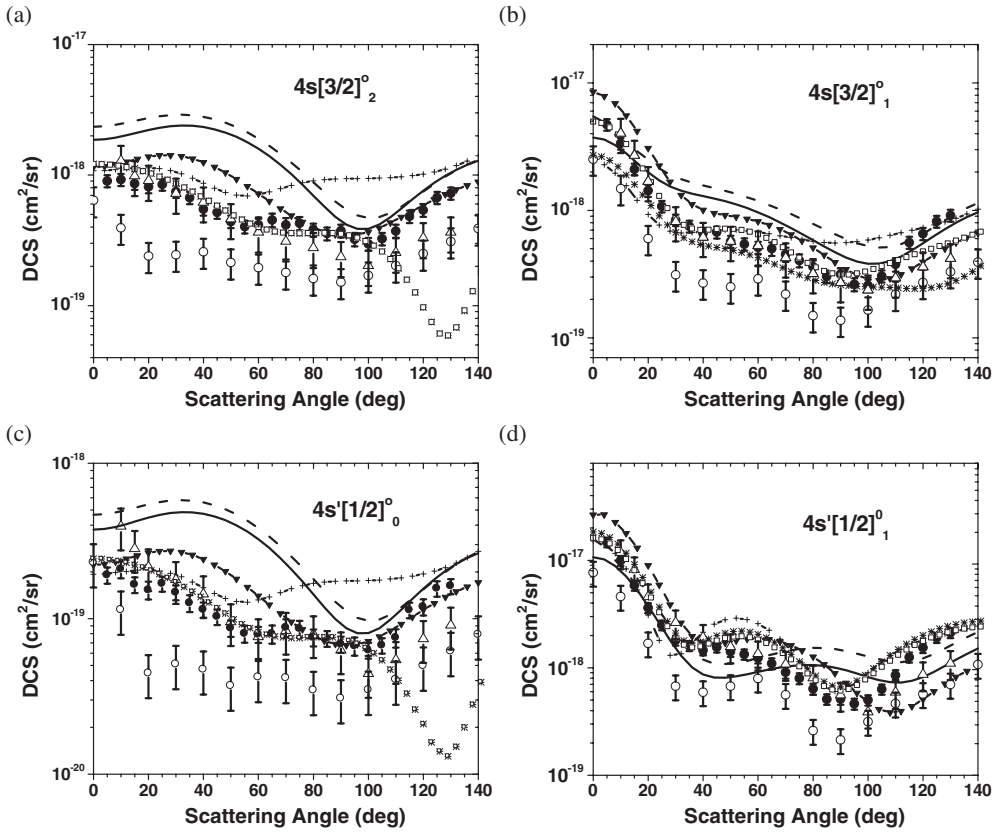

Figure 5. The same as figure 3, but for $E_0 = 20$ eV.

Figures 7(a)–(d) show DCSs at 50 eV. Here agreement between the experimental results and models for all levels is very good. Excellent agreement between our results and those of Chutjian and Cartwright (1981) is observed for the $(3p^5 4s')[1/2]^o_1$ level, however, the measurements of Filipovic *et al* (2000a) for this level show significant deviation from our measurements for $\theta < 40°$. The rise in the DCSs in the forward direction for the $(3p^5 4s)[3/2]^o_0$ level (figure 7(c)) is probably systematic and due to unfolding this weak feature from nearby strong dipole-accessible levels. The $(3p^5 4s)[3/2]^o_2$ level (which is not dwarfed by the strong dipole-accessible levels) does not display this forward peaking.

Figures 8(a)–(d) show DCSs at 100 eV. Apart from the $\theta = 10°$ point, our DCSs for all levels are in excellent agreement with the perturbative models. Excellent agreement between our experiment and that of Chutjian and Cartwright (1981) is also observed for the dipole-allowed levels. However, significant differences between our measurements and those of Chutjian and Cartwright (1981) exist for the metastable levels. Clearly, our results are in better agreement with the models for these transitions.

3.3. DCS ratios

We compare our experimental r, r' and r'' ratios to our calculations and to experimental ratios of Chutjian and Cartwright (1981), Filipovic *et al* (2000a, 2000b) and Khakoo *et al* (1994).

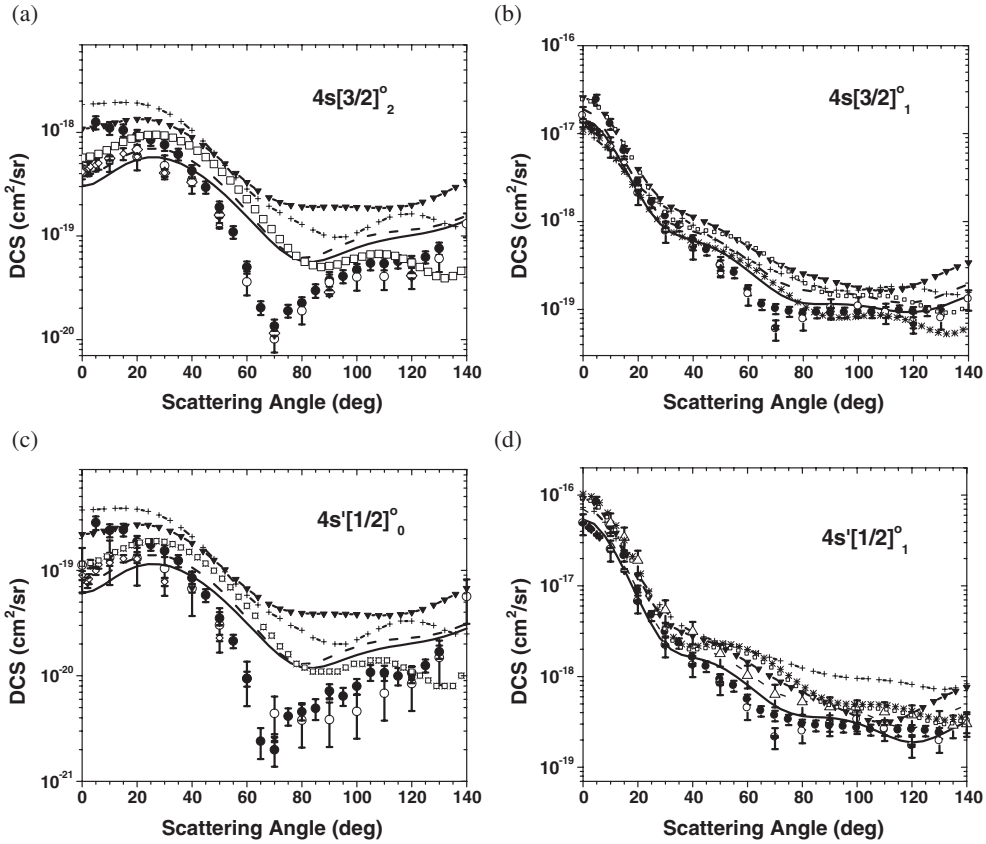

Figure 6. The same as figure 3, but for $E_0 = 30$ eV.

We note that these ratios are not affected by normalization to the elastic DCSs and are thus quantitatively more accurate than normalized DCSs.

(i) r: Figures 9(a)–(e) show r at different E_0 values. At $E_0 = 14$ and 100 eV, the uncertainty in r (which comprises the ratios of the weak metastable levels) is too large to make any meaningful comparisons with theory. This is because the DCSs for the metastable states are very small close to threshold and at high energies. Consequently, the measurements of these have proportionally larger statistical uncertainties.

At $E_0 = 15$ eV (figure 9(a)) the RM5/a calculations are in very good agreement with our r values. The measured average r is 5.4 ± 0.9 in excellent agreement with the statistical weight value of 5. However, we note the dip at small θ predicted by the RM5/a models.

At $E_0 = 17.5$ eV (figure 9(b)), we see a clear indication of the drop of r at $\theta < 15°$. Otherwise, for $\theta > 15°$ the value of r stays at 5 within small error bars. The drop in r is a possible indication of second-order effects (Khakoo *et al* 1994). It could also be a systematic problem in unfolding the weaker metastable features from the dipole-allowed features. This has to be investigated by a method that selectively detects the metastable levels, e.g. an electron-metastable coincidence method or similar. We also note that the RM5/a do not show this drop in r values at small θ. A similar observation as at 17.5 eV is seen at $E_0 = 20$ eV (figure 9(c)).

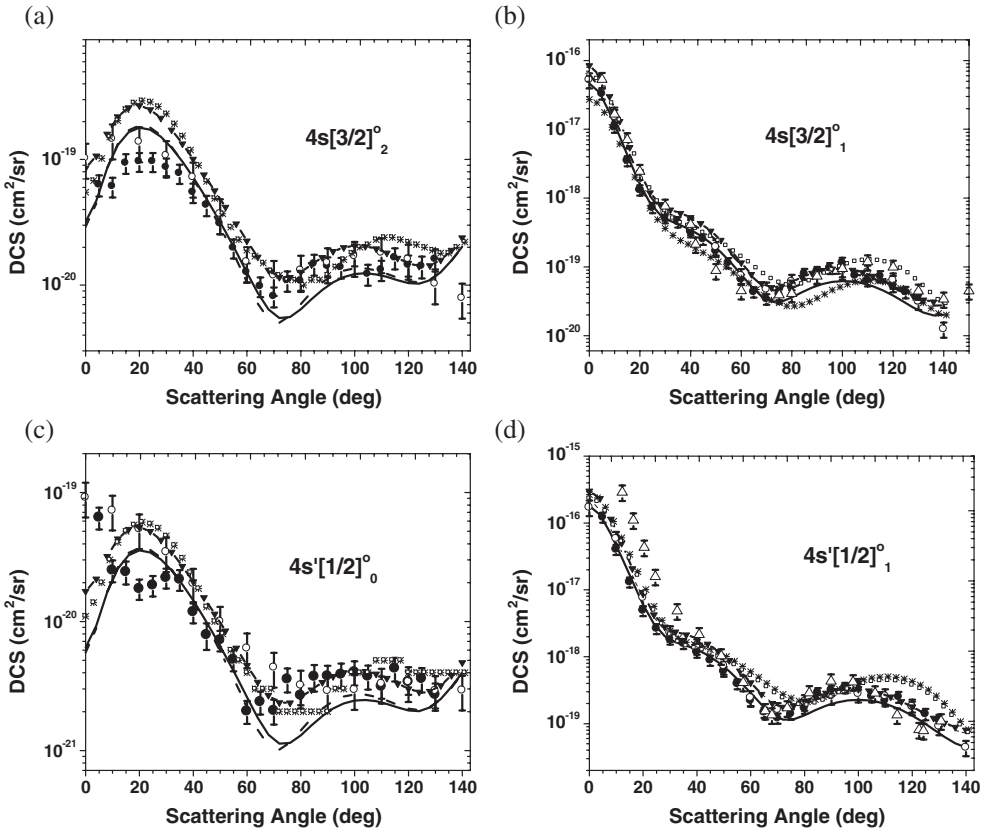

Figure 7. The same as figure 3, but for $E_0 = 50$ eV.

Here comparison with the r values of Chutjian and Cartwright (1981) and Filipovic *et al* (2000b) shows very good agreement. All experiments show a drop in r at small θ.

At $E_0 = 30$ eV (figure 9(d)), the previous forward angle drop in r seen at $E_0 = 17.5$ and 20 eV is not observed. We also note the rapid variation of r at angles about 70°. This is seen in the experimental results of Chutjian and Cartwright (1981) and somewhat less in ours. This variation shows the influence of the dip in the DCSs of the $J = 2$ and 0 levels at these θ. We also show previous r measurements taken by us Khakoo *et al* (1994) at this energy, which are in good agreement with the other experiments. All of the theories display r values that are very close to the statistical result.

At $E_0 = 50$ eV (figure 9(e)) r stays below the value of 5 and averages at 4.2 ± 0.8 for $\theta > 20°$. The r values of Chutjian and Cartwright (1981) follow the present results closely. At $E_0 = 100$ eV (not plotted here) the average r value is 4.5 ± 0.9, but the individual errors are very large. However the r ratios of Chutjian and Cartwright (1981) are very low, typically around 1.3. The models show r to be close to its statistical weight value at these high energies.

(ii) r': Figures 10(a)–(g) show the r' values at different E_0 values. The errors in r' are small because it constitutes the ratio between two strong transitions.

In figure 10(a) at $E_0 = 14$ eV, we observe considerable disagreement with theory. Our measurements show r' tending towards an extrapolated value of 0.43 ± 0.03 as $\theta \rightarrow 0$,

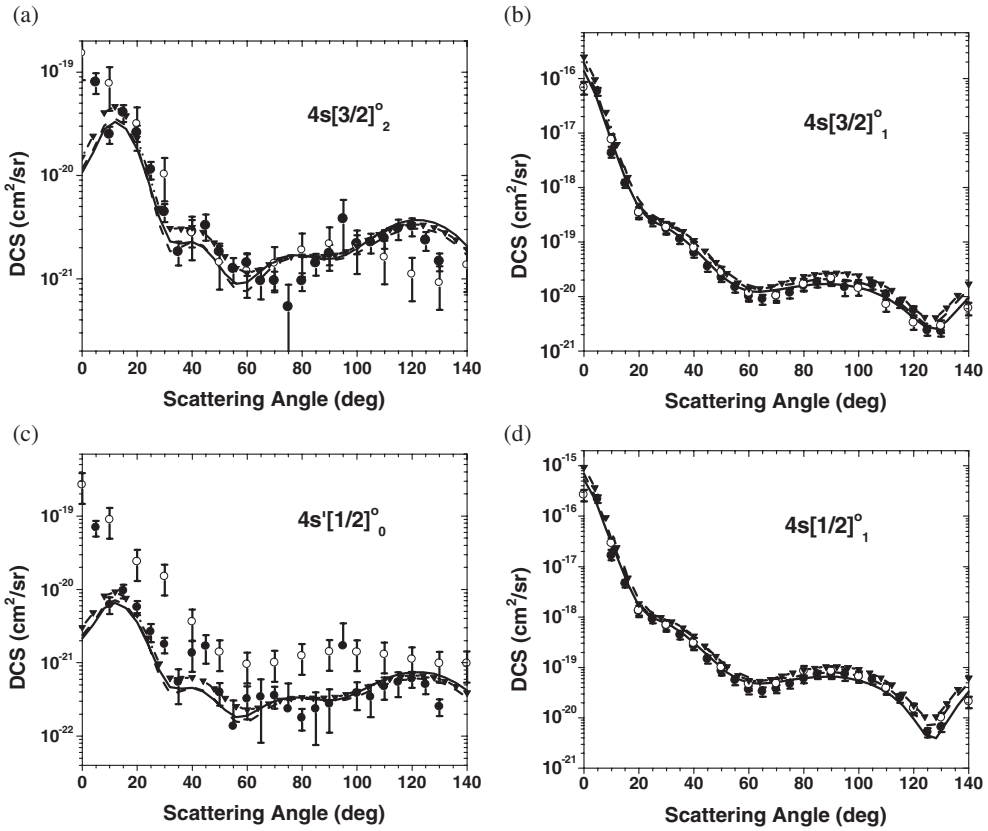

Figure 8. The same as figure 3, but for $E_0 = 100$ eV.

whereas theoretical values are significantly lower. The closest value of 0.35 is obtained by the UFOMBT. Our measurements indicate the presence of exchange at zero θ. At $\theta \approx 85°$, we note a broad r' maximum of $\approx$1 (increased spin-exchange), but theory either overestimates this (RM41) or both overestimates and places this maximum at higher θ.

At $E_0 = 15$ eV (figure 10(b)), the r' at this E_0 is similar to that of $E_0 = 14$ eV. This is contrary to the rapidly changing shapes of the DCSs (see section 3.2 and figures 3 and 4). At this energy, the r' tends toward an extrapolated value of 0.31 ± 0.01 as $\theta \to 0$. Agreement with theory is unsatisfactory, but is best with the UFOMBT in the small angle regime. We also note the oscillatory variation in r' as θ approaches the origin from $\theta = 90°$.

At $E_0 = 17.5$ eV (figure 10(c)), the r' ratio is similar to that of 15 eV, reaching a maximum of 0.8 at $\theta = 90°$. The extrapolated value of r' at $\theta = 0°$ is 0.292 ± 0.089. We also note a second weak maximum in r' at $\theta = 40°$, and observe a rapid decrease of r' from $\theta = 90°$ to 110°. The best agreement is observed with the RM5a, whereas the RM5 is in poor agreement. As opposed to the previous two incident electron energies, four of the theories do a reasonable job at predicting the limiting r' value as θ approaches zero.

At $E_0 = 20$ eV (figure 10(d)), the r' maximum at 40° is developed clearly and the larger maximum at $\theta = 90°$ is still present but is diminished in height to $\approx$0.6. The extrapolated r' value at $\theta = 0°$ is 0.310 ± 0.008. We note that RM5a gives better agreement than RM5 and locates both maxima as well as giving a good value of their magnitudes. The RM41

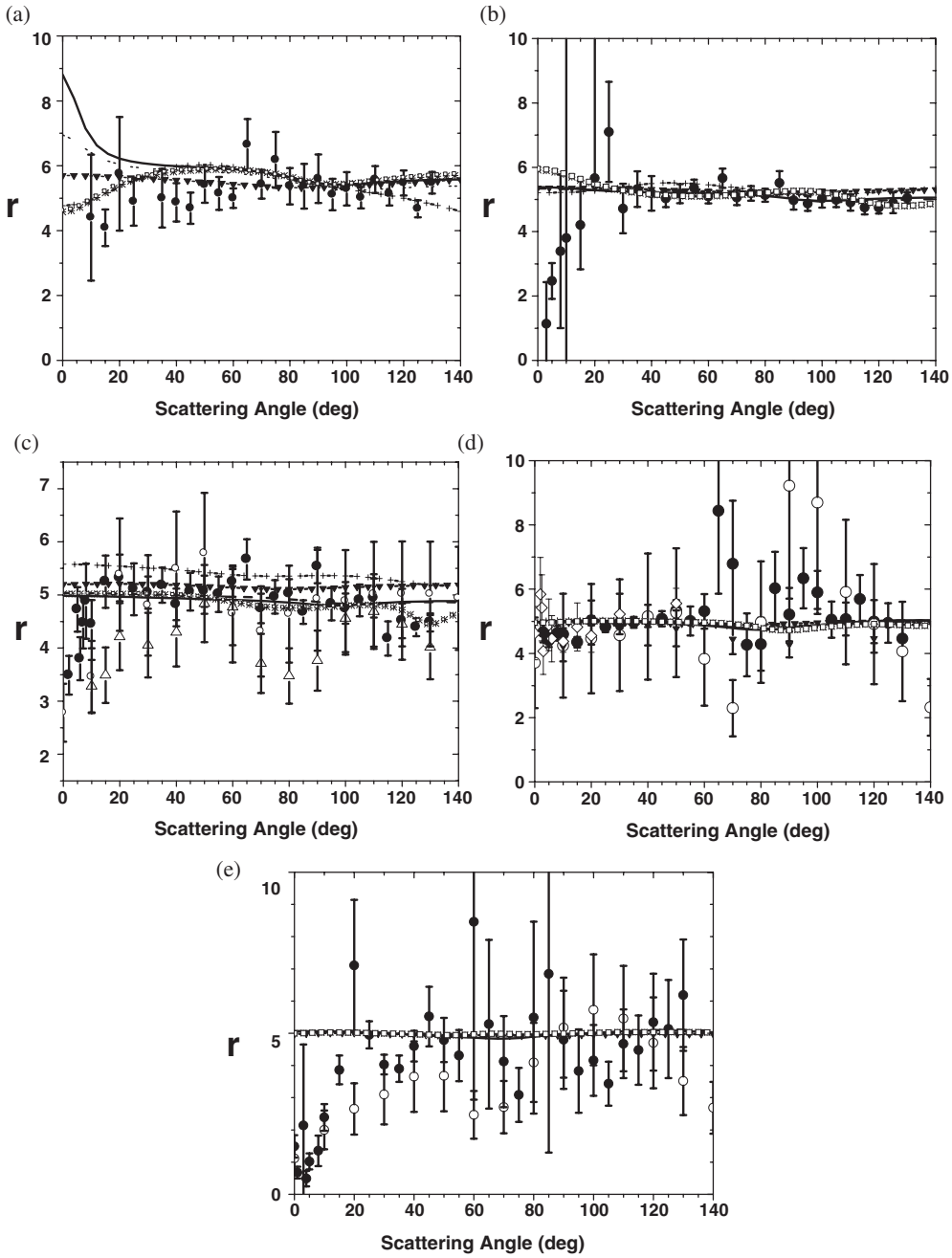

Figure 9. DCS ratio r as a function of E_0 and θ. The legend is the same as in figure 2. (a) $E_0 = 15$ eV, (b) $E_0 = 17.5$ eV, (c) $E_0 = 20$ eV, (d) $E_0 = 30$ eV and (e) $E_0 = 50$ eV. See also tables 2(a)–(g). For the metastable levels ($J = 2, 0$, figures (a) and (c)) the RM5a theory essentially equals RM5 for this feature. See the text for further discussion.

roughly locates these maxima, but exhibits sharpness in these maxima that is not observed experimentally. Good agreement with the r' values of the Chutjian and Cartwright (1981)

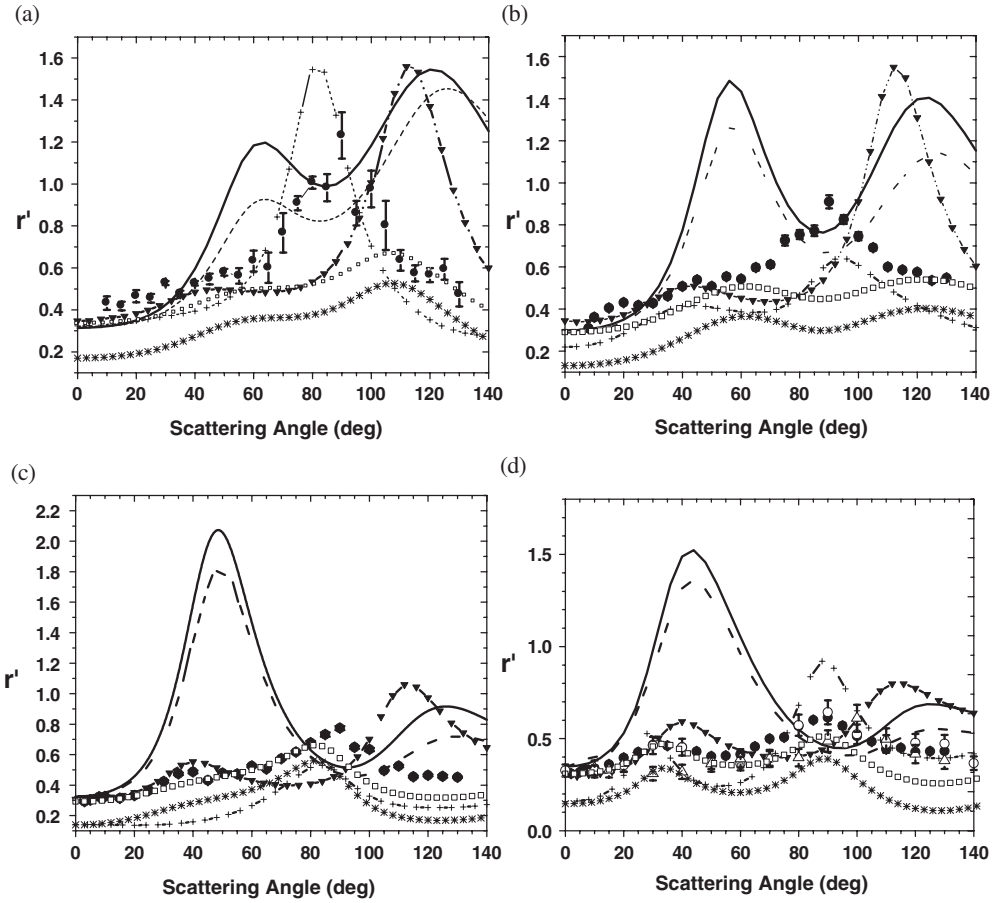

Figure 10. DCS ratio r' as a function of E_0 and θ. The legend is the same as in figure 2. (a) $E_0 = 14$ eV, (b) $E_0 = 15$ eV, (c) $E_0 = 17.5$ eV, (d) $E_0 = 20$ eV, (e) $E_0 = 30$ eV, (f) $E_0 = 50$ eV and (g) $E_0 = 100$ eV. See also tables 2(a)–(g).

measurements is observed except at $\theta = 70°$ where we suspect the steep minimum in the elastic DCSs may have affected their measurements to produce disagreement with our results. Surprisingly poor agreement with the measurements of Filipovic *et al* (2000a, 2000b) is observed except at small θ where they show excellent agreement with all experiments.

At $E_0 = 30$ eV (figure 10(e)), the r' maximum at 40° is clearly present while the maximum at $\theta = 90°$ has vanished. The extrapolated r' value at $\theta = 0°$ is 0.287 ± 0.001. Better agreement with the perturbative models (DWBA, RDWA, UFOMBT) is observed for small θ, but at larger θ (above 105°) the theories diverge from the experimental data. The RM5a shows the best agreement with experiment. We also see that agreement between experiments is excellent. Clearly the present measurements represent an improvement over past measurements including our earlier (1994) r' values.

At $E_0 = 50$ eV (figure 10(f)), the r' maximum at ≈40° has shifted into a smaller maximum at ≈30°. Good overall agreement with the perturbative models and the RM5a is observed. Whereas the $\theta = 30°$ maximum is obtained by the models, the other maxima are not. The extrapolated r' value at $\theta = 0°$ is 0.280 ± 0.0006. We note that the data of Chutjian

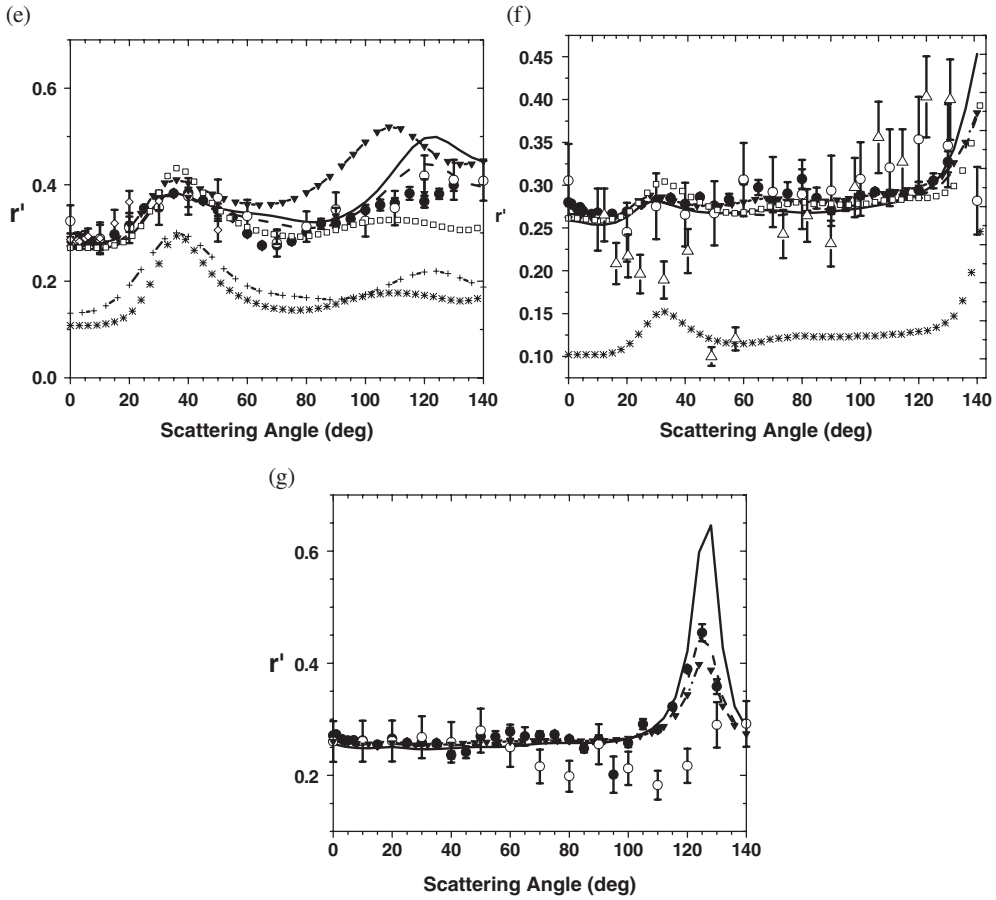

Figure 10. (Continued.)

and Cartwright (1981) show significantly more deviation than ours. Our experimental and theoretical data indicate the presence of a larger maximum around $\theta = 160°$.

At $E_0 = 100$ eV (figure 10(g)), a pronounced r' maximum of $\approx$0.45 at $\theta = 125°$ is observed and agreement with the models is excellent. The data of Chutjian and Cartwright (1981) miss this $\theta = 125°$ maximum and show considerable scatter at $\theta > 70°$. The extrapolated r' value at $\theta = 0°$ is at its most precise at 0.263 ± 0.001.

(iii) r'': Figures 11(a)–(g) show r'' at different E_0 values. In figure 11(a) at $E_0 = 14$ eV, we observe the best agreement with RM5 and RM5a and not with RM41. The perturbative theories show increased values of r'' as θ increases. At $E_0 = 15$ eV (figure 11(b)) the agreement with theory is much worse. None of the theories can reproduce the clear shape of r'' at $\theta > 40°$. At $E_0 = 17.5$ eV (figure 11(c)) the RM5a shows good agreement up to $\theta \approx 90°$, but then drops below the present experimental values. The RM5 is in lesser agreement with present results and the other theories do not show satisfactory agreement.

At $E_0 = 20$ eV (figure 11(d)), agreement with the r'' values of Chutjian and Cartwright (1981) is a little better than that of Filipovic *et al* (2000a, 2000b), especially around θ from 80° to 100° where the latter fall well below our r'' values. Agreement with RM5a is better than RM5

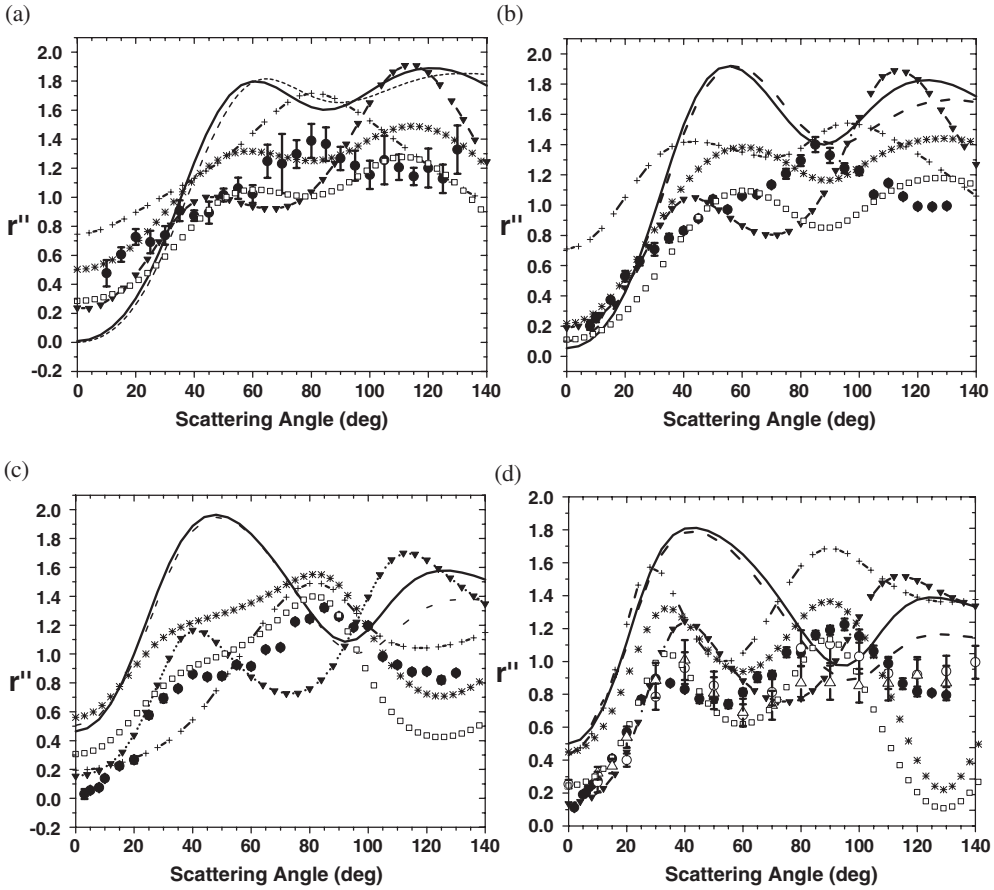

Figure 11. DCS ratio r'' as a function of E_0 and θ. The legend is the same as in figure 2. (a) $E_0 = 14$ eV, (b) $E_0 = 15$ eV, (c) $E_0 = 17.5$ eV, (d) $E_0 = 20$ eV, (e) $E_0 = 30$ eV, (f) $E_0 = 50$ eV and (g) $E_0 = 100$ eV. See also tables 2(a)–(g).

or RM41. However, the perturbative theories continue to show disagreement. At $E_0 = 30$ eV (figure 11(e)) agreement between our r'' values and those of Chutjian and Cartwright (1981) is excellent except around $\theta = 110°$. The best agreement is observed with the DWBA and RM5a. However, agreement with the other theories remains unsatisfactory. At this E_0 value, our experimental r'' values show a clear shape with r'' rising at $\theta \geqslant 130°$.

At $E_0 = 50$ eV (figure 11(f)), agreement with the perturbative theories is very good, where we see both experiments of Chutjian and Cartwright (1981) and the present results agreeing with the r'' values of the DWBA, UFOMBT and SCGS-RDWA calculations. We note that the DWBA is significantly lower than experimental r'' values around $\theta = 60°$. All of these models show the rise in r'' at around $\theta = 30°$, but overestimate this rise. At $E_0 = 100$ eV (figure 11(g)) agreement with all perturbative modes is excellent. We note that the SCGS-RDWA shows the best agreement especially at $\theta = 120°$ with r'' reaching high values, greater than 1. The experimental r'' values of Chutjian and Cartwright (1981) miss this rise of r'' around $\theta = 120°$. This rise is related to the increased DCS of the $(3p^5 4s)[3/2]_2^o$ level which is possibly related to an increase in spin-exchange (see also figure 10(g)).

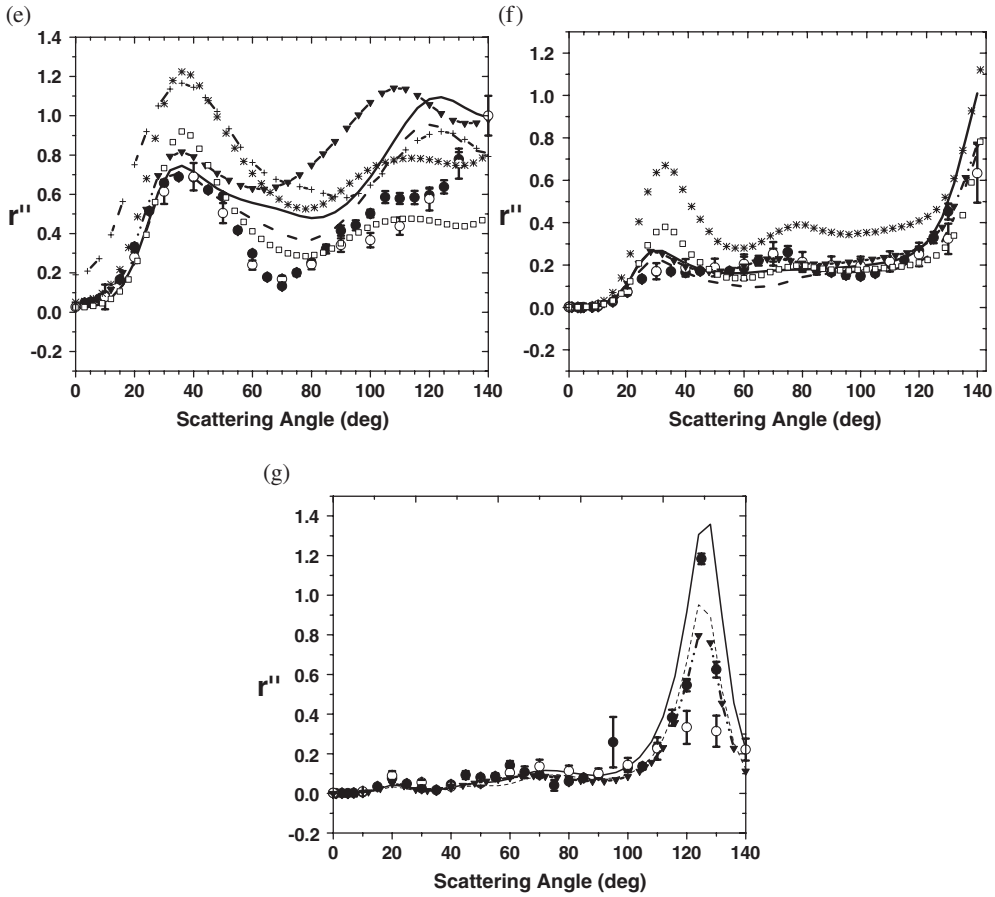

Figure 11. (Continued.)

3.4. Integral cross-sections

The experimental integral cross-sections (ICS) are summarized in table 4. Plots which also include the present theoretical ICSs from the *R*-matrix, DWBA, UFOMBT and SCGS-RDWA model are provided in figures 12(a) and (b) for the dipole-allowed $(3p^5 4s)[3/2]^o_1$ and $(3p^5 4s')[1/2]^o_1$ levels and in figures 13(a) and (b) for the dipole-forbidden $(3p^5 4s)[3/2]^o_2$ and $(3p^5 4s')[1/2]^o_0$ levels, respectively.

For the dipole-allowed levels, comparisons are made with the emission measurements of Ajello *et al* (1990) and the experimental ICSs of Chutjian and Cartwright (1981) and Filipovic *et al* (2000a, 2000b). Here the emission cross-sections of Ajello *et al* (1990) are in good qualitative agreement with the present ICSs, but had to be multiplied by factors of 0.29 and 0.55 for the $(3p^5 4s)[3/2]^o_1$ and $(3p^5 4s')[1/2]^o_1$ levels, respectively, in order to produce quantitative agreement with our measurements. This indicates (to some extent) the very large amount of cascade contributions to the emission signal. Comparison of the present measurements with the ICSs of Filipovic *et al* (2000a, 2000b) shows good agreement at $E_0 \leqslant 30$ eV, but shows increasing disagreement with our experiment for E_0 above 30 eV. The ICSs of Chutjian and Cartwright (1981) are in very good agreement with our measurements.

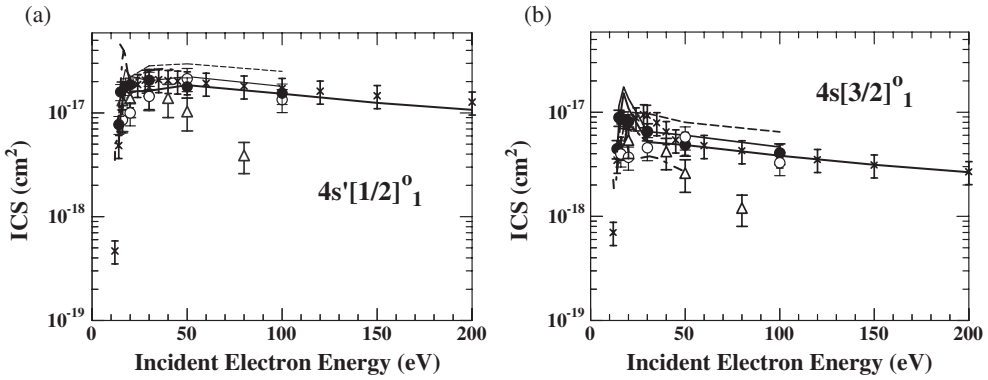

Figure 12. ICS for the optically allowed resonance transitions of Ar. (a) $(3p^5 4s)[3/2]^o_1$ feature and (b) $(3p^5 4s')[1/2]^o_1$ feature. Legend: Experiments: ●, present data; ○, Chutjian and Cartwright (1981); △, Filipovic *et al* (2000a, 2000b); × Ajello *et al* (1990), optical emission measurements ×0.55 for the $(3p^5 4s')[1/2]^o_1$ feature and ×0.29 for the $(3p^5 4s)[3/2]^o_1$ feature. The error bars in the emission measurements include their relative intensity error plus the error on the normalization to our ICSs (17% for (a) and 16% for (b)). Theories: —— DWBA; – – – UFOMBT; ——— SCGS-RDWA (thicker line); - —- RM41; - - —- - RM5, 5a.

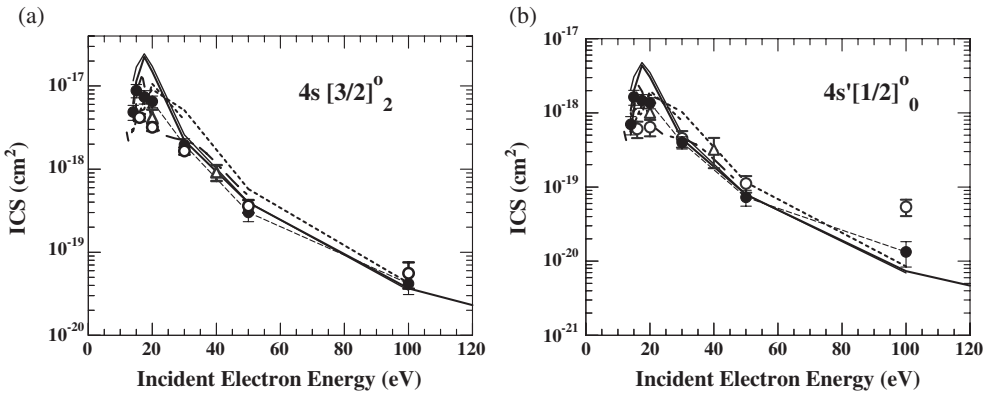

Figure 13. ICS for the optically forbidden transitions of Ar. The legend is the same as in figure 12. (a) The $(3p^5 4s)[3/2]^o_2$ feature. (b) The $(3p^5 4s')[1/2]^o_0$ feature.

Table 4. ICS with corresponding uncertainties (1 standard deviation) for the individual $3p^5 4s$ excitations of Ar obtained by angle-integrating the measured DCSs in table 2. Units: cm^2.

E_0 (eV)	$4s[3/2]^o_2$	Error	$4s[3/2]^o_1$	Error	$4s'[1/2]^o_0$	Error	$4s'[1/2]^o_1$	Error	r (integral)	Error
14	4.86E−18	9.92E−19	4.45E−18	8.95E−19	6.98E−19	1.93E−19	7.72E−18	1.51E−18	7.0	2.4
15	8.81E−18	1.59E−18	8.88E−18	1.57E−18	1.64E−18	3.75E−19	1.59E−17	2.82E−18	5.4	1.6
17.5	7.42E−18	1.36E−18	8.50E−18	1.55E−18	1.46E−18	3.08E−19	1.80E−17	3.28E−18	5.1	1.4
20	6.53E−18	1.04E−18	8.14E−18	1.29E−18	1.37E−18	2.32E−19	1.87E−17	2.94E−18	4.8	1.1
30	1.96E−18	3.59E−19	6.52E−18	1.21E−18	4.00E−19	7.51E−20	2.07E−17	3.87E−18	4.9	1.3
50	3.02E−19	6.89E−20	4.86E−18	1.07E−18	7.26E−20	1.76E−20	1.78E−17	3.93E−18	4.2	1.4
100	4.18E−20	1.08E−20	4.06E−18	9.13E−19	1.33E−20	5.00E−21	1.55E−17	3.47E−18	3.1	1.4

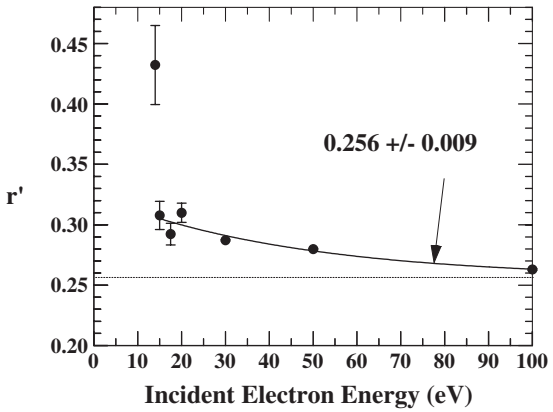

Figure 14. E_0 dependence of r' ($\theta \rightarrow 0$) showing extrapolation of r' to the dipole limit of $\theta \rightarrow 0$, $E_0 \rightarrow \infty$, using an exponential function. The dipole limit of r' determined from the exponential extrapolation is 0.256 ± 0.009, as shown. See also table 5.

For the metastable levels (figures 13(a) and (b)), we compare with the ICSs of Chutjian and Cartwright (1981) and Filipovic *et al* (2000b). For both levels, we note the well-defined shape in the present results which are in very good agreement with the results of Chutjian and Cartwright and Filipovic *et al*, showing disagreement with our ICSs only at $E_0 = 100$ eV for the $(3p^5 4s')[1/2]_0^o$ level (figure 13(b)).

We note that it would be useful to carry out an apparent generalized oscillator strength (AGOS) extrapolation for the dipole-allowed transitions. However, we did not perform very small $\theta < 10^\circ$ measurements in this case at the highest E_0 values of 50 and 100 eV. Thus, AGOS fits (see Khakoo *et al* (2002) for details of such fits) were found not to extrapolate reliably to the $K^2 \rightarrow 0$ regime, where K is the momentum transfer.

3.5. r' extrapolations to determine α, β parameters

Figure 14 shows our $\theta \rightarrow 0^\circ$ extrapolated r' values at different E_0 values fitted to an exponential function (excluding the very high r' value at $E_0 = 14$ eV), that extrapolates to $r' = 0.256 \pm 0.009$ at large E_0. Using this r' value, and the relationship $\alpha^2 + \beta^2 = 1$, we were able to calculate α and β parameters which are shown in table 5. We note the overall excellent agreement with r' from recent OOS measurements. These α and β parameters can be used as a check for theoretical models in the future, and thus the present experiment gives an example of the usefulness of electron scattering measurements for atomic spectroscopy.

4. Conclusions

We have presented accurate experimental DCSs and DCS ratios for the excitation of the $3p^5 4s$ configuration of Ar over a large range of impact energies and thereby improved the experimental situation that existed before our measurements. However, there still remain disagreements between theory and experiment, especially at low energies. Theoretical modelling of electron scattering from the rare gases is difficult because of the complexity of representing the role of the (correlated) core electrons and the fact that the excited states are no longer LS-coupled states. The present work shows clearly that accurate representation of the target wavefunction is necessary for progress to be made. We observe excellent agreement between the perturbative

Table 5. Experimental OOS values (au) for the singlet states of the $3p^5 4s$ configuration of Ar, the dipole limit of r' determined from these OOS values, and the corresponding α and β parameters (and uncertainties) obtained from r'. See the text for further discussion. See Chan *et al* (1992) for a more extensive summary of optical measurements.

$2p^5 3s[3/2]_1^o$	$2p^5 3s[1/2]_1^o$	r'	Reference	Method	α	β
		0.256 ± 0.009	Present	Electron energy loss	0.892 ± 0.003	0.451 ± 0.006
0.0662 ± 0.0033	0.265 ± 0.013	0.2498 ± 0.0175	Chan *et al* (1992)	High resolution dipole (e, e)	0.894 ± 0.006	0.447 ± 0.013
0.057 ± 0.003	0.213 ± 0.011	0.2676 ± 0.0197	Tsurubuchi *et al* (1989)	Absolute self-absorption	0.888 ± 0.007	0.459 ± 0.013
0.0580 ± 0.0030	0.222 ± 0.02	0.2613 ± 0.0271	Li *et al* (1988)	Electron energy loss	0.890 ± 0.010	0.455 ± 0.019
0.063 ± 0.005	0.24 ± 0.02	0.2625 ± 0.0302	Westerveld *et al* (1979)	Absolute self-absorption	0.890 ± 0.011	0.456 ± 0.021
0.066 ± 0.005	0.255 ± 0.02	0.2588 ± 0.0282	Geiger (1992)	Electron energy loss	0.891 ± 0.010	0.453 ± 0.020

theories and the experimental DCSs and DCS ratios at $E_0 \geqslant 50$ eV. We find, contrary to our expectations, that the present experimental DCSs and DCS ratios show increasing disagreements with theories at E_0 values of 30 eV and below. Clearly, the use of OOS-based α, β parameters yields improved results as demonstrated in the case of the RM5a over the RM5. We note that the UFOMBT and DWBA calculations were also improved when the OOS-based α and β parameters were used. The fact that r' is able to provide information which leads to an improvement of wavefunctions is very important, but this information can only be used directly in the case of simple wavefunctions. For more complex multi-configuration wavefunctions, the experimental r' values can be used as an important check on the accuracy of the calculations. It would also be useful to make more precise measurements of r, especially at small θ, to investigate the reduction of this parameter by possible second-order effects. Presently we are considering the method of electron-metastable coincidence or a similar method to accomplish this.

Acknowledgments

This work was funded by the National Science Foundation under Grants No RUI-PHY-9731890 (MAK, JGC and PV), PHY-0070872 (DHM) and PHY-0244470 (KB). Authors RS and SS are thankful to Council of Scientific and Industrial Research (CSIR), New Delhi, for sanctioning their grant to support the present research. ADS wishes to thank the Natural Sciences and Engineering Research Council of Canada for a grant in aid of this research. Discussions with Professor T J Gay (University of Nebraska, Lincoln) are gratefully acknowledged.

References

Ajello J Jr, James G K, Franklin B and Howell S 1990 *J. Phys. B: At. Mol. Opt. Phys.* **23** 4355
Andersen N and Bartschat K 2001 *Polarization, Alignment, Orientation in Atomic Collisions* (New York: Springer)
Bartschat K and Madison D H 1987 *J. Phys. B: At. Mol. Phys.* **20** 5839
Bartschat K and Madison D H 1992 *J. Phys. B: At. Mol. Opt. Phys.* **25** 4619
Bartschat K and Zeman V 1999 *Phys. Rev.* A **59** R2552
Becker K, Crowe A and McConkey J W 1992 *J. Phys. B: At. Mol. Opt. Phys.* **25** 3885
Chan W F, Cooper G, Guo X, Burton G R and Brion C E 1992 *Phys. Rev.* A **46** 149
Childers J G, James K E, Hughes M, Bray I, Baertschy M and Khakoo M A 2003 Low energy electron impact of atomic hydrogen: I. Ionization *Phys. Rev.* A submitted
Chutjian A and Cartwright D C 1981 *Phys. Rev.* A **23** 2178
Corr J J, van der Burgt P J M, Plessis P, Khakoo M A, Hammond P and McConkey J W 1991 *J. Phys. B: At. Mol. Opt. Phys.* **24** 1069
Corr J J, Wang S and McConkey J W 1992 *J. Phys. B: At. Mol. Opt. Phys.* **25** 4929
Dubois R D and Rudd M E 1976 *J. Phys. B: At. Mol. Phys.* **9** 2657
Dümmler M, Hanne G F and Kessler J 1995 *J. Phys. B: At. Mol. Opt. Phys.* **28** 2985
Filipovic D M, Marinkovic B P, Pejcev V and Vuskovic L 2000a *J. Phys. B: At. Mol. Opt. Phys.* **33** 677
Filipovic D M, Marinkovic B P, Pejcev V and Vuskovic L 2000b *J. Phys. B: At. Mol. Opt. Phys.* **33** 2081
Furst J E, Golden D E, Magerefteh M, Zhou J and Mueller D 1989 *Phys. Rev.* A **40** 5592
Geiger J 1992 unpublished observations as quoted in Chan *et al*
Guo X, Khakoo M A, Mathews D J, Mikaelian G, Crowe A, Kanik I, Trajmar S, Zeman V, Bartschat K and Fontes C J 1999 *J. Phys. B: At. Mol. Opt. Phys.* **32** L155
Hibbert A 1975 *Comput. Phys. Commun.* **9** 141
Khakoo M A, Beckmann C E, Trajmar S and Csanak G 1994 *J. Phys. B: At. Mol. Opt. Phys.* **27** 3159
Khakoo M A and McConkey J W 1986 *Phys. Rev. Lett.* **57** 679
Khakoo M A and McConkey J W 1987 *J. Phys. B: At. Mol. Phys.* **20** 5541
Khakoo M A, Wrkich J, Larsen M, Kleiban G, Kanik I, Trajmar S, Brunger M J, Teubner P J O, Crowe A, Fontes C J, Clark R E H, Zeman V, Bartschat K, Madison D H, Srivastava R and Stauffer A D 2002 *Phys. Rev.* A **65** 062711
Li G P, Takayanagi T, Wakiya K, Suzuki H, Ajiro T, Yagi S, Kano S S and Takuma H 1988 *Phys. Rev.* A **38** 1240

Madison D H, Maloney C M and Wang J B 1998 *J. Phys. B: At. Mol. Opt. Phys.* **31** 873
Martus K E, Zheng S H and Becker K 1991 *Phys. Rev.* A **33** 1682
Meneses G D, Csanak G and Cartwright D C 1991 *Proc. 17th Int. Conf. on the Physics of Electronic and Atomic Collisions* ed I E McCarthy, W R MacGillivray and M C Standage (Brisbane: Griffith University Press) p 129 (Abstracts)
Meneses G D, da Paixao F J and Padial N T 1985 *Phys. Rev.* A **32** 1956
Moore C E 1952 *Atomic Energy Levels* NBS Circular no 467 (Washington DC: US Government Printing Office)
Nickel J C, Zetner P W, Shen G and Trajmar S 1989 *J. Phys. E: Sci. Instrum.* **22** 730
Panajotovic R, Filipovic D, Marinkovic B, Pejcev V, Kurepa K and Vuskovic L 1997 *J. Phys. B: At. Mol. Opt. Phys.* **30** 5877
Parpia F A, Froese-Fischer C and Grant I P 1996 *Comput. Phys. Commun.* **94** 249
Srivastava S K, Tanaka H, Chutjian A and Trajmar S 1981 *Phys. Rev.* A **23** 2156
Tsurubuchi S, Watanabe K and Arikawa T 1989 *J. Phys. B: At. Mol. Opt. Phys.* **22** 2969
Westerveld W B, Mulder Th F A and Van Eck J 1979 *J. Quant. Spectrosc. Radiat. Transfer* **21** 533
Williams J F 1979 *J. Phys. B: At. Mol. Phys.* **12** 265
Zheng S H and Becker K 1993 *J. Phys. B: At. Mol. Opt. Phys.* **26** 517
Zuo T, McEachran T and Stauffer A D 1992 *J. Phys. B: At. Mol. Opt. Phys.* **25** 3393